SEISMIC DECONVVOLUTION BASED ON FRACTIONALLY INTEGRATED NOISE

by

Muhammad M. Saggaf

B.S., King Fahd University of Petroleum and Minerals (1989)

Submitted to the Department of Earth, Atmospheric and Planetary Sciences
in partial fulfillment of the requirements for the degree of

Master of Science

at the

MASSACHUSETTS INSTITUTE OF TECHNOLOGY

April 1996

Signature of Author _____
Department of Earth, Atmospheric and Planetary Sciences
April 1996

Certified by _____
M. Nafi Toksöz
Professor of Geophysics
Thesis Supervisor

Accepted by _____
Thomas H. Jordan
Chairman
Department of Earth, Atmospheric and Planetary Sciences

SEISMIC DECONVVOLUTION BASED ON FRACTIONALLY INTEGRATED NOISE

by

Muhammad M. Saggaf

Submitted to the Department of Earth, Atmospheric and Planetary Sciences
on April 1995, in partial fulfillment of the
requirements for the degree of
Master of Science

Abstract

Seismic deconvolution is nowadays, and has been for some time, an integral part of geophysical data processing. The objective of seismic deconvolution is to recover the earth's reflectivity from the seismic trace by removing the effects of source reverberations. The most widely-used deconvolution method is by far that based on Weiner filtering. The conventional implementation of this method assumes that the earth's reflectivity series is modeled by a white noise process, in order to make the problem of calculating the deconvolution filter more tractable. However, the earth's reflectivity is observed to have power spectra that are actually proportional to frequency; in other words, to have a richer content of high frequency, or to exhibit blueness.

In this thesis we propose to model reflection coefficients by a process that mimics the behavior observed of the earth more closely than white noise. This process is called fractionally integrated noise, and is defined as the process whose fractional differencing gives rise to white noise. The stochastic properties of fractionally integrated noise approximate those observed of data derived from typical well logs much better than random white noise. For instance, the power spectrum is proportional to frequency, and the auto correlation function falls off less rapidly than a unit pulse.

We develop an efficient method for modifying the conventional Weiner deconvolution scheme to use fractionally integrated noise and do away with the assumption of white noise. The method is implemented in such a way that the computational overhead is minimal and that it is a generalization of the conventional method, so that it reduces to the conventional scheme when the

underlying fractionally integrated noise process reduces to white noise. Also, the proposed implementation can be thought of as a preliminary filter that corrects for blueness; and in this case deconvolution methods other than Weiner filtering can be used in its second stage. We analyze the computational requirements for the proposed implementation and also suggest ways to estimate the parameter of the underlying process.

We study the effectiveness of the generalized deconvolution based on fractionally integrated noise by applying it to synthetic traces derived from real well log data and comparing its output to the exact reflection coefficients used to produce the synthetic traces. We also compare it to the outcome obtained from applying the conventional Weiner deconvolution method. The results are quite favorable and show the generalized method to have a clear edge over the conventional method. The generalized method also appear to be quite robust in the sense that it outperforms the conventional method over a wide range of the estimate of the underlying process parameter.

Thesis Supervisor: M. Nafi Toksöz
Title: Professor of Geophysics

TABLE OF CONTENTS

LIST OF FIGURES

ACKNOWLEDGMENTS

I would like to thank my advisor, Nafi Toksöz, for his guidance, advice, and feedback – at both the academic and personal levels – throughout my stay at MIT. His support of his students and dedication goes beyond duty, and is unparalleled.

My thanks also go to Ernest Shtatland for introducing me to self-similar processes in geophysics, and for numerous lively and enjoyable discussions about fractals in natures, from which this research had its roots. I am also thankful to Sven Treitel for the very useful course he taught on seismic deconvolution at ERL.

I would like to thank Ted Madden for his helpful input and being always glad to discuss my ideas, Michel Bouchon for teaching me to discrete wavenumber theory and applications to cracked media, Roger Turpening for helping with the data and lending me his books on deconvolution, and to Batakrishna Mandal and Bill Rodi for very useful discussions about seismic inversion.

My gratitude also goes to Sadi Kuleli for being the friend that he is and for making my stay away from home more pleasant, and to my office-mate for two years, Joe Matarese, who was always helpful with assistance about geophysics, computers, and mixing those two together.

My sincere thanks also go Jane Maloof and the ERL staff, especially Liz Henderson, Sue Turbank and Naida Buckingham. I would also like to thank my fellow students at ERL. I would especially like to mention Rick Bennet, Ted Charrette, Ningya Cheng, Wenjie Dong, Rick Gibson, Matthijs Haartsen, Burc

Oral, Richard Patterson, Chengbin Peng, Arcangelo Sena, Delaine Thompson, and Xiaomin Zhao.

It goes without saying that everything that I am, or will ever be, I owe to my family. My parents have always been supportive of me, and I value their devotion and trust immensely.

In short, I would like to thank everybody for everything! I think that sums it up pretty well.

The author was supported by ARAMCO during his graduate school tenure at MIT when this work was carried out.

INTRODUCTION

Objective

The purpose of this thesis is to develop a generalization of the conventional Weiner deconvolution based on a statistical process that mimics the earth's behavior more closely than the current widely-used models based on the assumption of white noise randomness. We present both the theoretical background and practical analysis of this approach.

Seismic Deconvolution – Background

In petroleum explorations, a seismic source imparts an acoustic wave that travels into the subsurface formations. Part of the energy of the wave reflects at each interface with an acoustic impedance contrast and part is transmitted through the rock layers. The recorded trace can be thought of as the composition of many identically-shaped seismic wavelets arriving at the recording instrument at varying times and with varying amplitudes. These times and amplitudes, in other words the form of the trace, are governed by the structure of the underlying earth surfaces. The sequence of numbers representing this structure is called the earth's reflectivity series, or the series of reflection coefficients.

In one dimension, the observed seismic trace can be represented as the convolution of the source function (i.e. the seismic pulse) with the reflectivity function. The objective of seismic deconvolution is to recover the reflectivity behavior of the earth from the recorded trace by removing the wavelet

components. Today, seismic deconvolution is a fundamental element of every geophysical data processing scheme in petroleum exploration.

By far the most widely used method of calculating the deconvolution filter is Weiner filtering (Peacock and Treitel, 1968). Among the other methods are l_1 norm criterion (Barrodale and Roberts, 1973), Burg's method (Burg, 1975), Kalman filtering (Ott and Meder, 1972; Crump, 1974), minimum entropy deconvolution (Wiggins, 1978 and 1985), homomorphic deconvolution (Ulrych, 1971; Buttkus, 1975), zero-phase deconvolution and time-adaptive algorithms (Clarke, 1968; Griffiths *et al.*, 1977). Jurkevics and Wiggins (1984) compared these methods and concluded that Weiner filters are the most robust under a wide variety of input conditions. Weiner deconvolution is sometimes also called least-squares inverse filtering.

Conventional deconvolution schemes assume that the earth's reflectivity has a white noise correlation structure. However, reflection coefficients in nature tend to behave in a different manner: generally their power spectra are proportional to frequency (Hosken, 1980; Walden and Hosken, 1985; Todoeschuck *et al.*, 1990; Rosa and Ulrych, 1990).

Figures 1, 2, and 3 show the power spectra of typical reflectivity logs from three different wells. The spectra were calculated by FFT analysis on the samples using the Welch method of power spectrum estimation and a Hanning window. Note how each spectrum has a richer content of high frequencies (this is sometimes referred to as "blueness"), and appears to have a direct proportional relation to frequency. Such behavior is encountered quite frequently in nature, and has been noted over the years. This is sometimes

described as quasi-cyclic and blocky layering and can be interpreted as evidence of self-organization and structuring in the crust (Shtatland, 1991). We will examine two of these wells later on when we analyze the effectiveness of the new method.

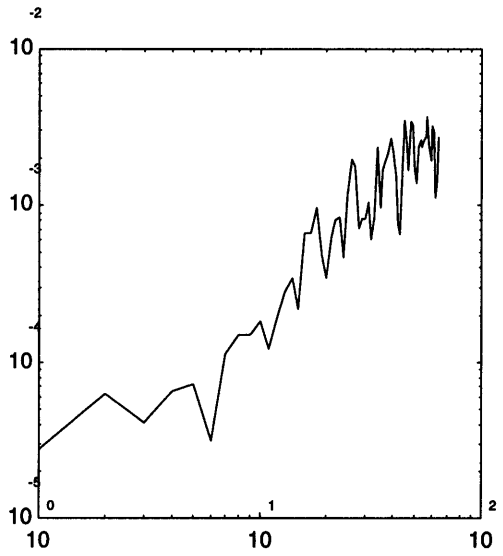

Figure 1: Example of power spectrum of reflectivity derived from well logs for the Ste. Helene well described later in the thesis.

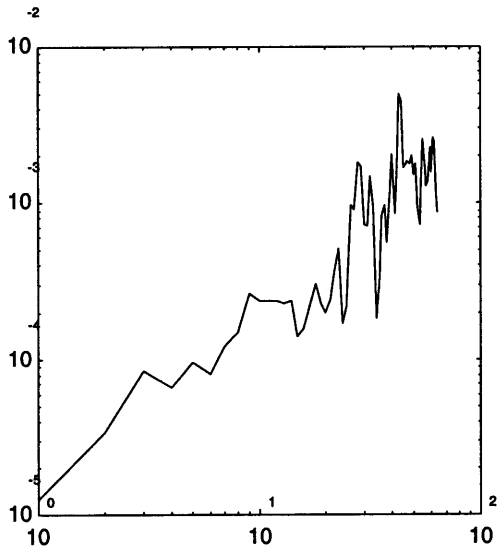

Figure 2: Example of power spectrum of reflectivity derived from well logs for the Wickham well described later in the thesis.

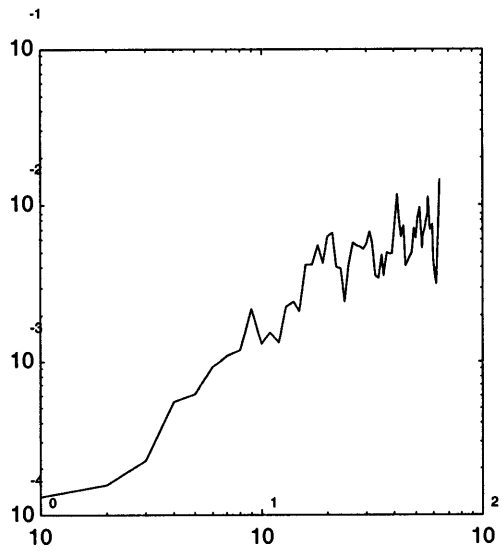

Figure 3: Example of power spectrum of reflectivity derived from well logs for the Puffin well (Canada).

The observations made above suggest that we can improve on the conventional Weiner deconvolution scheme by taking into account the behavior of reflectivity noted above; in other words, by discarding the white noise assumption, and modeling the earth by a process that emulates it better. The goal here then is to generalize the conventional Weiner deconvolution procedure to take into account the non-white-noise randomness behavior of the earth's structure, and to do that in an efficient and robust manner.

Several other issues related to deconvolution in general are worth noting here. For example, the amplitude and frequency content of the source wavelet are always affected by depth attenuation, the wavelet may have lateral variations, it may not be minimum-phase, the reflectivity series may not be stationary or Gaussian, and the trace is almost always encumbered by incoherent ambient noise from wind motion or the recording instrument. These issues, as well as suggested solutions for them (e.g. spherical divergence correction, exponential gain, time-gate processing, application of an inverse Q-filter, ..etc.), have been extensively studied in numerous papers and most standard textbooks (Claerbout, 1976; Mendel, 1983; Ziolkowski, 1984; Yilmaz, 1987), and will not be discussed here.

Outline

In the following chapters, we first begin by a quick review of the white noise process, and then introduce and define the fractionally integrated noise approach. We give examples of synthesized samples using various parameters and show typical power spectrum and auto-correlation functions for each process.

We then give a brief description of the conventional Weiner deconvolution, and go on to describe the scheme proposed to generalize this

technique using fractionally integrated noise. Some qualitative assessment of the new method's robustness and efficiency, as well as suggestions for estimating the process parameter, are discussed as well.

In the final chapter we perform some tests of the new scheme using real data and compare it to the conventional method. Data from two well logs are utilized in these tests, and two methods for evaluating the results are presented.

The appendices contain mathematical developments of the tools and concepts described in the thesis, as well as the code for the more essential computer programs used.

FRACTIONALLY INTEGRATED NOISE – STATISTICAL BACKGROUND

A process $\{z_t\}$ is said to be white noise if it consists of uncorrelated random variables. The auto-correlation function of such a process is a simple unit spike (Priestly, 1981),

$$\rho_z(k) = \delta_{0,k} \tag{1}$$

The process can be Gaussian, but does not have to be so, i.e. being white noise is a description of the correlation structure of the process, not the probability distribution structure. White noise is sometimes also called "random noise" or "random orthogonal series".

Figure 4 shows a typical synthetic realization of a white noise process (synthesizing a realization is discussed in some detail in Appendix A). The process in this figure is normalized to have zero mean and unit variance. Figures 5 and 6, respectively, show the power spectrum and auto-correlation function of this realization, along with the theoretical graphs of these functions (shown by the dotted lines). The theoretical and sample power spectrum and auto-correlation function are in good agreement given the size of the sample (the reader is reminded that a sample stochastic property will not in general be an exact match to the theoretical one unless the whole *ensemble* of the process is considered, rather than a single realization).

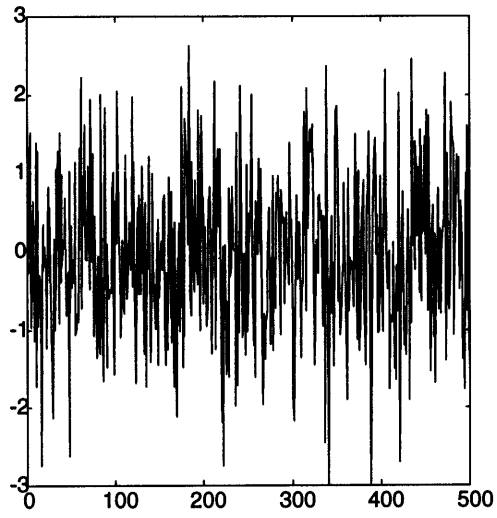

Figure 4: Synthesized realization of a white noise process. The process is normalized to have zero mean and unit variance.

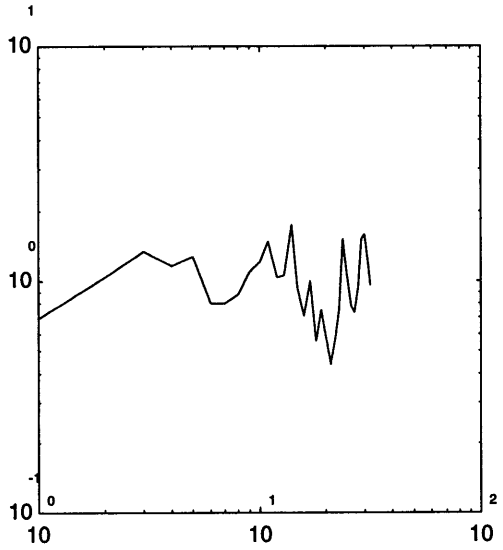

Figure 5: Power spectrum of the above process. The dotted line indicates the theoretical power spectrum of a white noise process.

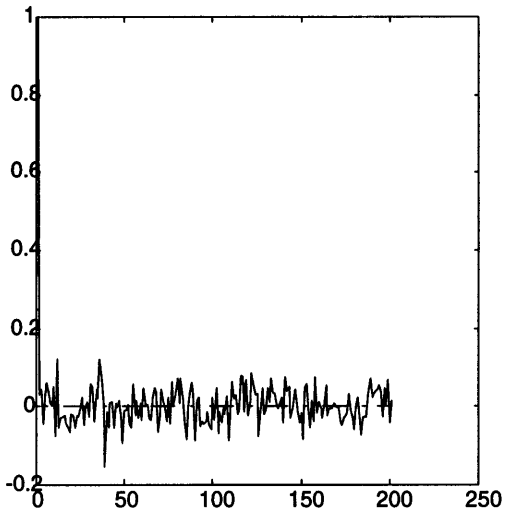

Figure 6: Auto-correlation function of the above synthesized sample. The dotted line indicates the theoretical auto-correlation function of a white noise process

Fractionally Integrated Noise

A process $\{y_t\}$ is said to be fractionally integrated noise of order d (we'll denote it sometimes by FIN, or FIN(d)) if its dth differencing is white noise (Hosking, 1981 and 1984). This may be written as $\nabla^d y_t = z_t$, where $\{z_t\}$ is a white noise process and ∇ is the differencing operator. ∇^d can in turn be defined by $\nabla^d = (1-B)^d$, where B is the background shift operator: $By_t = y_{t-1}$. d in this definition need not be an integer, and the process is stationary for $d < 0.5$. $\{y_t\}$ is Gaussian if $\{z_t\}$ is so. Notice that $d = 0$ corresponds to the case of white noise (i.e. zero differencing).

The auto-correlation function and power spectrum of this process are given by

$$\rho_y(k) = \frac{\Gamma(1-d)\Gamma(k+d)}{\Gamma(d)\Gamma(k+1-d)} \tag{2}$$

$$P_y(f) = \sigma^2\sqrt{\pi}\frac{\Gamma(1-d)}{\Gamma(\frac{1}{2}-d)}\sin^{-2d}(\pi f) \tag{3}$$

where σ^2 is the variance of $\{z_t\}$ (Hosking, 1981 and 1984). (Unlike the formula given by Hosking, however, the power here is normalized so that the process has unit variance).

Figures 7 through 13 show several synthetic realizations of fractionally integrated noise processes of varying order d. In these figures, d has values of -1.0, -0.75, -0.5, 0, 0.25 -0.4 and 0.48, respectively. Notice how the process starts to depart from being stationary as the order approaches 0.5 (which is the threshold). Also note that figures 4 and 10 are identical, since in the case of $d = 0$, the fractionally integrated noise process reduces to white noise (zero differencing). The same random seed was used to generate those two figures.

Appendix A describes a method of producing synthetic realizations of a fractionally integrated noise process of a given order. The appendix also contains the computer code used to generate the samples in this section.

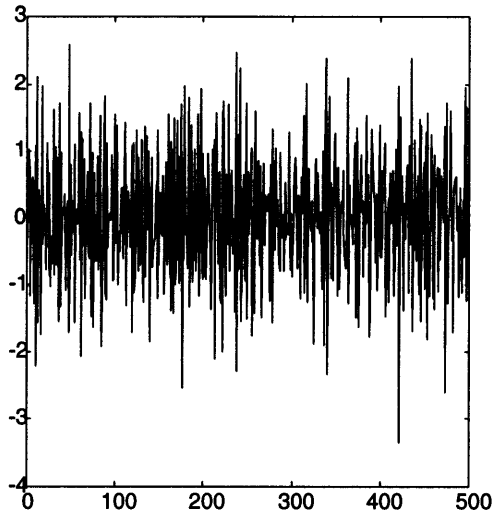

Figure 7: Synthesized realization of a fractionally integrated noise process of order d = -1.0. The process is normalized to have zero mean and unit variance.

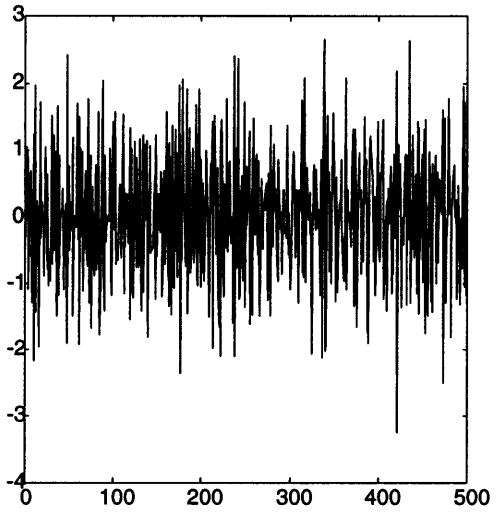

Figure 8: Synthesized realization of a fractionally integrated noise process of order d = -0.75

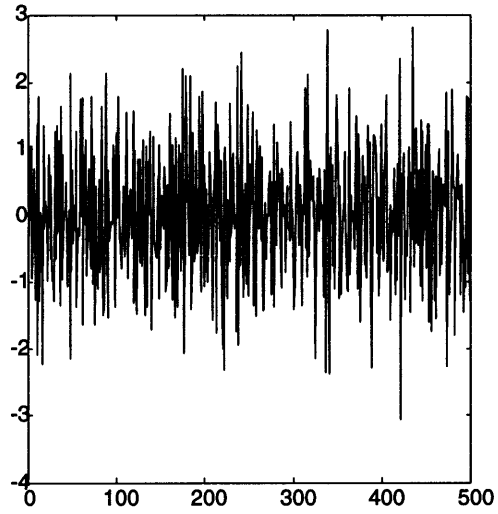

Figure 9: Synthesized realization of a fractionally integrated noise process of order d = -0.5.

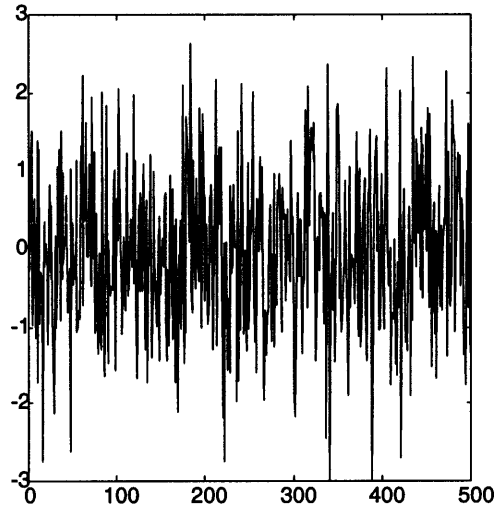

Figure 10: Synthesized realization of a fractionally integrated noise process of order d = 0.

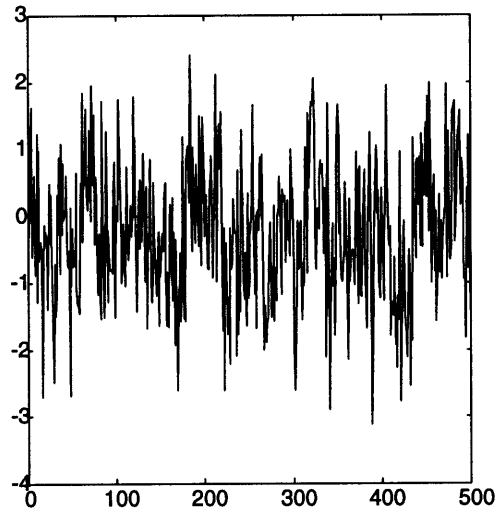

Figure 11: Synthesized realization of a fractionally integrated noise process of order d = 0.25.

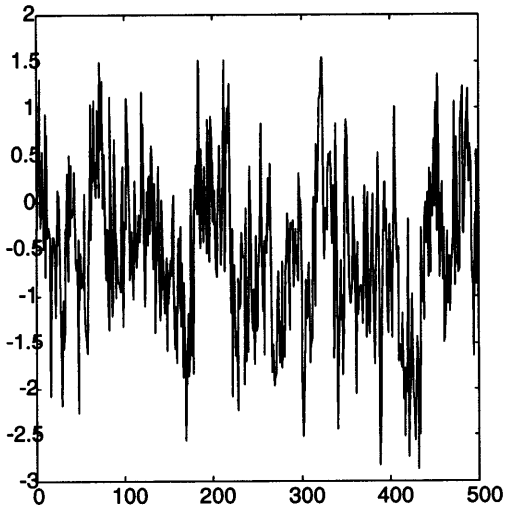

Figure 12: Synthesized realization of a fractionally integrated noise process of order d = 0.4.

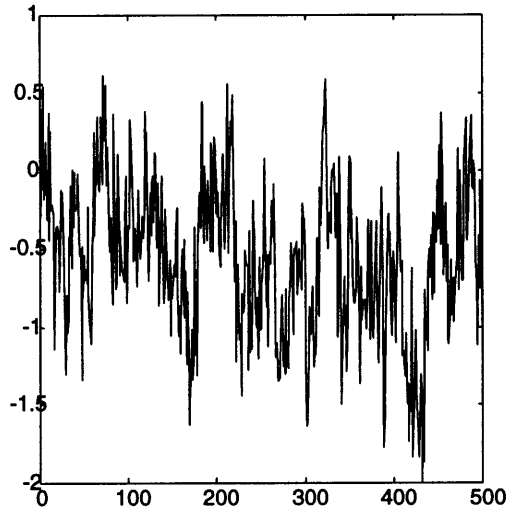

Figure 13: Synthesized realization of a fractionally integrated noise process of order d = 0.48.

Figures 14 and 15, respectively, show the power spectrum and auto-correlation function of the realization shown in figure 8 (i.e. when $d = -0.75$), along with the theoretical graphs of these functions at the same process order (shown by the dotted lines). Of particular interest is that the power spectrum is not simply a flat line like that of random white noise, but is rather proportional to frequency – just as observed of the earth's behavior (see figures1–3). Also note that the auto-correlation function falls off less quickly than that of random noise, indicating that this process has somewhat of a longer memory (or more persistence) than white noise.

From (3) we see that for $d = 0$, the power spectrum is independent of frequency (white noise); and for $d > 0$, the power is inversely proportional to frequency (figure 16 shows the power spectrum of the fractionally integrated noise process of order 0.4, whose realization was depicted in figure 12). Thus, in modeling the earth's reflection coefficients, we are interested only in the

fractionally integrated noise processes whose order $d \leq 0$, typically in the range (-1, 0).

Figure 17 shows the auto-correlation function of fractionally integrated noise at the first three lags plotted versus the order of the process d. Notice how the correlation is identically zero at $d = 0$ (white noise) and how the process approaches non-stationarity at the upper end of the range of the process order. For $d < 0$, the auto-correlation function falls off very rapidly as the lag increases.

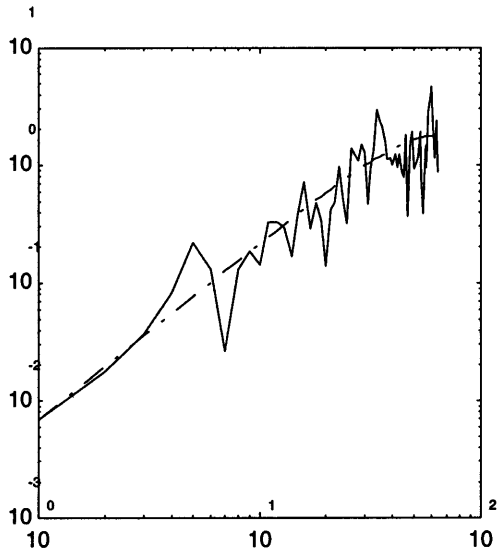

Figure 14: Power spectrum of the process depicted in figure 8. The dotted line shows the theoretical power spectrum of a normalized fractionally integrated noise process of order -0.75.

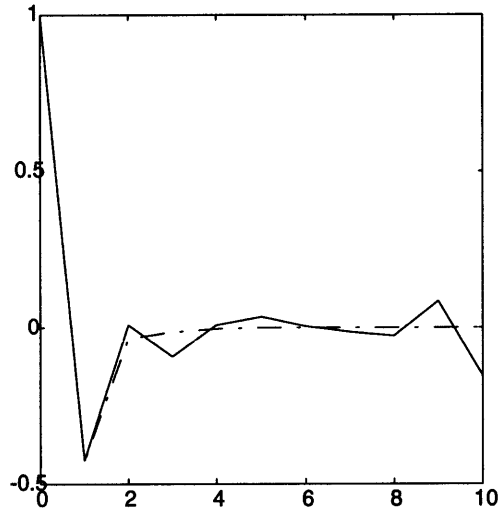

Figure 15: Auto-correlation function of the process depicted in figure 8. The dotted line shows the theoretical auto-correlation function of a normalized fractionally integrated noise process of order -0.75.

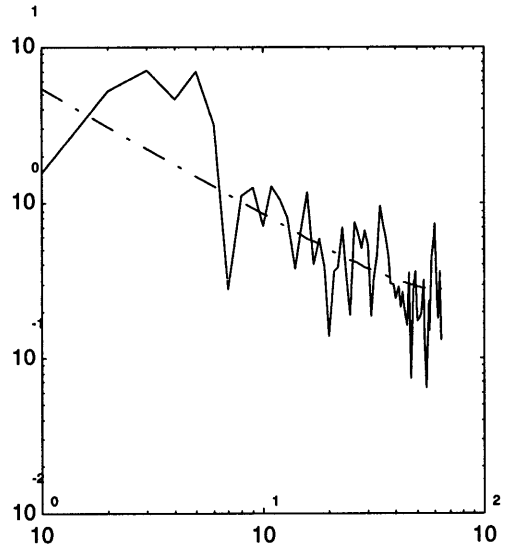

Figure 16: Power spectrum of the process depicted in figure 12. The dotted line shows the theoretical power spectrum of a normalized fractionally integrated noise process of order 0.4.

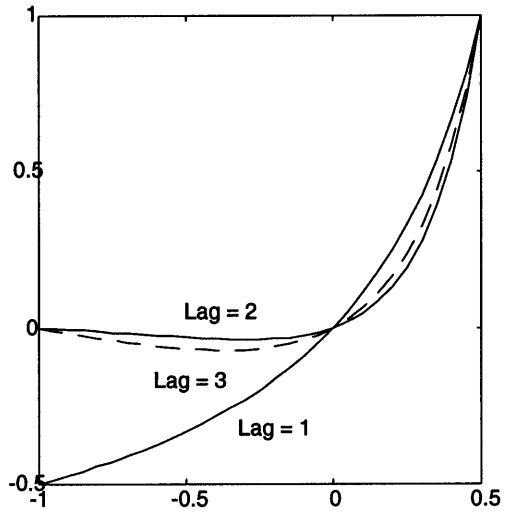

Figure 17: Auto-correlation of fractionally integrated noise at the first three lags plotted versus the order of the process d.

Parameter Estimation for the Order of the Process

For any given data sample, the order d of the fractionally integrated noise process can be found in either the frequency or time domains. In the frequency domain, the order of the process can be calculated by a least-squares fit of the theoretical power spectrum of the process as given by equation (3) to that of the data. In Appendix B we give the mathematical derivation and analysis for this scheme, as well as describe its implementation. Figures 18, 19 and 20, respectively, depict the power spectra of the best-fitting fractionally integrated noise processes found using this method for the data examples whose spectra were shown on figures 1, 2 and 3.

Furthermore, since the auto-correlation function of the fractionally integrated noise process is easily calculable analytically, fitting can also be done in the time domain using stochastic time-series analysis. This is especially useful

if the process is to be generalized and thought of as a FARIMA(p,d,q) process, i.e. a fractionally-integrated auto-regressive moving-average process (and therefore, a fractionally integrated noise process is the special case FARIMA(0,d,0)). The computations can done, for example, by modifying the procedure given by Box and Jenkins (1976) for the ARIMA(p,d,q) process slightly to take into account the fact that the parameter can be a fraction and perform the differencing accordingly. Hosking (1984) also gives a maximum-likelihood method for performing the calculations. There is little evidence, however, that such higher orders of approximation are warranted, given the uncertainty in the parameters of such estimates.

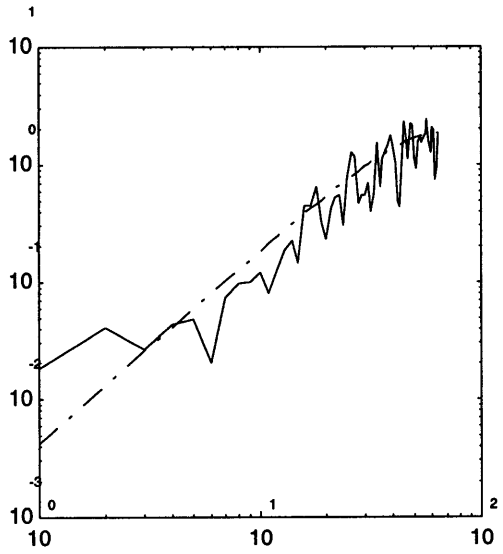

Figure 18: The dotted line shows the power spectrum of the best-fitting fractionally integrated noise process (d = -0.82) to that of the data of figure 1. The solid line shows the power spectrum of the data.

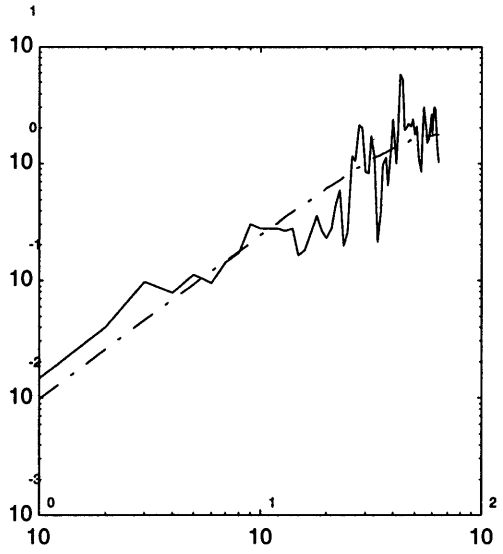

Figure 19: Power spectrum of the data in figure 2 (solid line) and best-fitting fractionally integrated noise process (d = -0.70) to that of the data (dotted line).

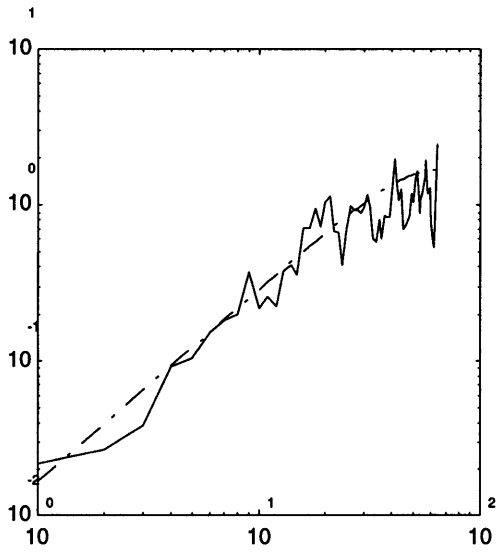

Figure 20: Power spectrum of the data in figure 3 (solid line) and best-fitting fractionally integrated noise process (d = -0.62) to that of the data (dotted line).

GENERALIZING WEINER DECONVOLUTION

As we mentioned earlier, the seismic trace can be thought of as the composition of several identically-shaped wavelets arriving at varying times and with varying amplitudes, as governed by the earth's reflectivity. Let's suppose that the shape of the wavelet, which we will assume to be causal and minimum-delay, is given by the sequence $w = (w_0, w_1, \ldots, w_n)$. Figure 21 shows a simple wavelet of length 3 consisting of $w = (w_0, w_1, w_3)$. Figure 22 shows three wavelets of this shape arriving at times t, $t-1$ and $t-2$, and whose amplitudes are weighed by $r_t = 1.5$, $r_{t-1} = 1.0$ and $r_{t-2} = 0.5$, respectively.

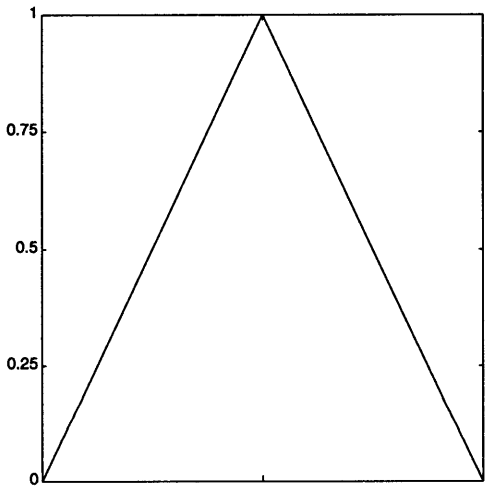

Figure 21: Simple wavelet of length 3

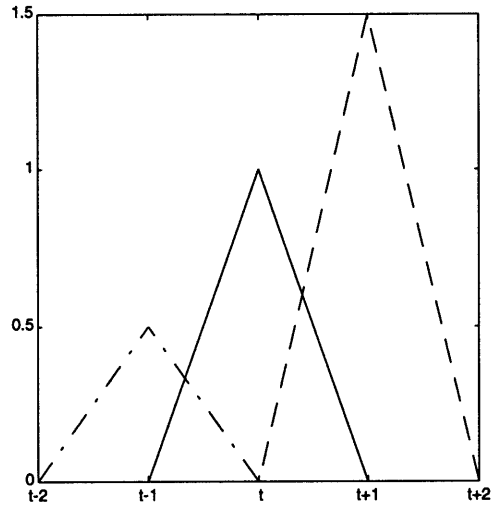

Figure 22: Three simple wavelets arriving at varying times and with varying amplitudes.

Thus, the value of the trace at time t is made up of the contribution $w_0 r_t$ from the wavelet that arrived at time t, the contribution $w_1 r_{t-1}$ from the wavelet that arrived at time $t-1$ and the contribution $w_2 r_{t-2}$ from the wavelet that arrived at time $t-2$. So the trace at time t can be written as

$$\begin{aligned} s_t &= w_0 r_t + w_1 r_{t-1} + w_2 r_{t-2} \\ &= \sum_{k=0}^{2} w_k r_{t-k} \end{aligned} \tag{4}$$

In general, for a wavelet of length n+1, we can represent the value of the trace at time t by

$$s_t = \sum_{k=0}^{n} w_k r_{t-k} \tag{5}$$

This is called the convolution of w and r, and we can now write the trace as the convolution of the wavelet and reflectivity

$$s = w * r \tag{6}$$

where * denotes the convolution operator.

The goal in deconvolution is to develop a filter f such that when applied to the trace, it recovers the earth's reflectivity behavior. This problem has been studied extensively in reflection seismology (Robinson and Treitel, 1980; Mendel, 1983; Yilmaz, 1987). In Appendix C we present a brief discussion for the reader's convenience. To recover reflectivity from the trace by removing the wavelet, we have to solve the system of normal equations

$$\mathbf{A}_w f = \delta \tag{7}$$

where $\mathbf{A}_w$ is the Toeplitz matrix consisting of the auto-correlation values of the wavelet, and $\delta = (1,0,\ldots,0)^T$. The resulting filter represents the inverse of the wavelet, such that when applied to the trace, it gives

$$\begin{aligned} f * s &= f * (w * r) \\ &= (f * w) * r \\ &= r \end{aligned} \tag{8}$$

and hence the reflection coefficients are recovered.

We note, however, that since the auto-correlation function of the wavelet is unknown, the matrix $\mathbf{A}_w$ is unknown, and it is therefore not possible to calculate the above filter without additional information.

Conventional Weiner Deconvolution

Conventional deconvolution schemes get around the above dilemma by modeling reflectivity by white noise. The auto-correlation function of the wavelet (ϕ_{ww}) would then be equal to that of the trace (ϕ_{ss}), and thus we have

$$\phi_{ss}(k) = \phi_{ww}(k) \tag{9}$$

which means that

$$\mathbf{A}_s = \mathbf{A}_w \tag{10}$$

and the equation (7) thus reduces to

$$\mathbf{A}_s f = \delta \tag{11}$$

In this case, the auto-correlation values in $\mathbf{A}_s$ are those of the trace, and they can be readily calculated from the seismic trace. The conventional Weiner deconvolution operator f is therefore found by solving the set of normal equations (11).

Generalized Weiner Deconvolution Using Fractionally Integrated Noise

Wiener deconvolution can be generalized to take into account the non-white noise behavior of reflectivity. In this case we do not assume that reflectivity has a white noise correlation structure. Instead, we model reflectivity by a fractionally integrated noise process, which mimics the earth's behavior to a much closer extent than white noise. Then we make use of the fact that inverse least-squares filters can be used to spike (up to a constant multiple) any signal of known auto-correlation function.

Assume that we modeled reflectivity by a fractionally integrated noise process of order d. The auto-correlation function of reflectivity can then be found from (2), and a filter g can be designed to spike reflectivity out of the trace. This can be done by solving the normal equations

$$\mathbf{A}_r g = \delta \tag{12}$$

Applying g to the trace gives (using (6))

$$\begin{aligned} \hat{s} &= g * s \\ &= s * g \\ &= (w * r) * g \\ &= w * (r * g) \\ &= w \end{aligned} \tag{13}$$

The result $\hat{s} = g * s$ therefore has the same auto-correlation function as the wavelet, and (7) reduces to

$$\mathbf{A}_{\hat{s}} f = \delta \tag{14}$$

The deconvolution filter f can hence be found by solving this system of equations. Here, $\mathbf{A}_{\hat{s}}$ consists of the auto-correlation values of the output of the filter g, and those can be calculated after applying the filter to the trace.

For $d = 0$, $\mathbf{A}_r = I$, and g becomes the identity filter. The resulting deconvolution filter in this case is then exactly the conventional Weiner deconvolution filter described in the previous section. Thus, the conventional Weiner deconvolution is a special case of the generalized one, just as white noise is a special case of fractionally integrated noise.

To summarize, in order to calculate the generalized deconvolution filter, we perform the following procedure (computer code for implementing this method is given in Appendix C):

1. Assume an underlying fractionally integrated process for reflectivity.
2. Calculate the auto-correlation coefficients of this process from (2) to generate $\mathbf{A}_r$.
3. Solve the set of normal equations (12) to produce the filter g.
4. Apply the filter g to the trace.
5. Apply the conventional deconvolution method to the output of the filter found in the previous step.

This method can hence also be thought of as a preliminary step that corrects for blueness in reflectivity (i.e. the non-white-noise behavior of having a richer content of high frequency in the power spectrum) and prepares the trace for the normal deconvolution process. Considered in this manner, the method has the advantage that any deconvolution method can be used in the second stage of the process after the correction filter is applied, and one is not really limited to using Weiner deconvolution.

In practice, the reflection coefficients are unknown, and so is the value of the order of the process, d. The use of the above deconvolution scheme can then be achieved in two ways:

- By using a value of d obtained from a nearby well.
- By experimenting with different values of d and choosing the one that gives the best output (e.g. sharper events, ...etc.)

If data from nearby wells are available, the first approach for obtaining d is the preferred one.

Use of the above options requires that the generalized deconvolution filter be relatively insensitive to the choice of the order of the process, d. It would also be very useful if the generalized deconvolution filter could consistently outperform the conventional ones over a pre-determined range of the values of d, so that even a poor choice of d would still give better results than the conventional filter. As can be seen in the examples, the generalized deconvolution filter seems to have both the above merits.

An Efficient Method for Implementation

Todoeschuck and Jensen (1988) proposed a scaling Gaussian noise deconvolution that is computed recursively by solving a system of equations based on a Toeplitz matrix at each iteration. To reduce the number of calculations at each iteration, as well as the recursion level, only the values of the auto-correlation function of the process at the first two lags were used, and the values in the rest of the sequence were set to zero. They noted that the solution converges satisfactorily after a small number of iterations, typically less than 10.

The number of calculations required to solve a system of equations based on a Toeplitz matrix of size $n \times n$ (where n is the length of the filter) using the Levinson algorithm (see Appendix C) is proportional to n^2 (Robinson and Treitel, 1980). Hence, calculating the conventional Weiner deconvolution filter requires about n^2 calculations, and the method suggested by Todoeschuck and Jensen (1988) requires about $10 \cdot n^2$ calculations. In other words, it requires about an order of magnitude more computations than conventional filtering. Furthermore, making use of values of the auto-correlation function at higher lags would, in general, require more iterations.

If the size of the filter is comparable to the number of iterations, the amount of calculations needed is roughly the same as that of solving the system by reducing the matrix instead of using Levinson recursion, since in both cases the number of calculations required would be about n^3. The matrix needs to be reduced only once since it stays the same through all iterations, and only back-substitution is needed at each stage.

Conversely, the method of calculating the generalized deconvolution filter based on fractionally integrated noise as proposed in this thesis requires solving the systems (12) and (14) only once. Thus, the overhead over conventional deconvolution is that of solving a set of normal equations based on a Toeplitz matrix only once; which, as we mentioned above, is about n^2 calculations. In other words, finding the generalized deconvolution filter using this method requires a number of calculations of *the same* order of magnitude as that of computing the conventional deconvolution filter (it is roughly equivalent to calculating the conventional filter twice, as can be seen from the above discussion).

This is a much more efficient scheme than that of Todoeschuck and Jensen (1988). Moreover, is has the advantages that none of values of the auto-correlation function of the process is discarded (and thus it is more exact), it does not suffer from any convergence difficulties for problematic wavelets, and the type of deconvolution used in the second stage of the scheme need not be based on Weiner filtering. In other words, the filters in the two stages of the method are decoupled.

EXAMPLES AND ANALYSIS

Data Source

Here we use reflectivity series derived from sonic logs of two wells: the Soquip Ste. Helene and the Shell Wickham No. 1, both located in St. Lawrence Lowlands of Quebec. These data were supplied by Dr. John Todoeschuck. The reflection coefficients were calculated from the sonic logs using the usual formula:

$$r = \frac{v_2\rho_2 - v_1\rho_1}{v_2\rho_2 + v_1\rho_1} \approx \frac{v_2 - v_1}{v_2 + v_1} \tag{15}$$

where v is the velocity, and the density ρ was assumed to be constant with depth.

We'll start with the Ste. Helene well. Its reflection coefficients are shown on figure 23 (in this figure, as well as other subsequent time-series plots, the x-axis represents normalized time). The power spectrum of this reflectivity series appears on figure 24, along with that of the best-fitting fractionally integrated noise process (shown by the dotted line), which was found to be $d = -0.82$ in this case.

To contrast the two deconvolution schemes, a source wavelet, figure 25, is convolved with the reflectivity series of the well to produce a synthetic trace, shown on figure 26. The deconvolution filters are then applied to the trace and the outputs are compared to the true reflection coefficients.

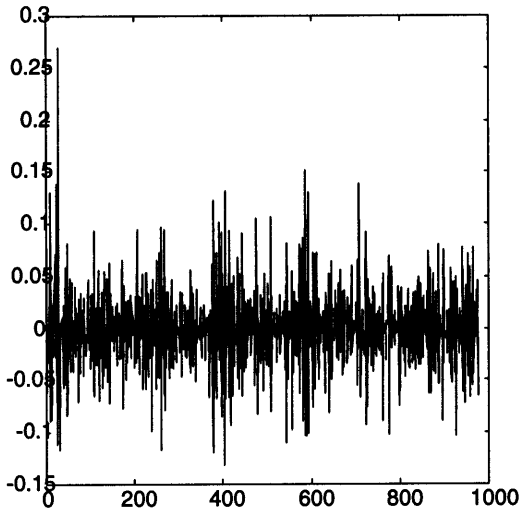

Figure 23: Reflection coefficients of the Ste. Helene well. The x-axis in this figure, as well as other subsequent time-series plots, represents normalized time.

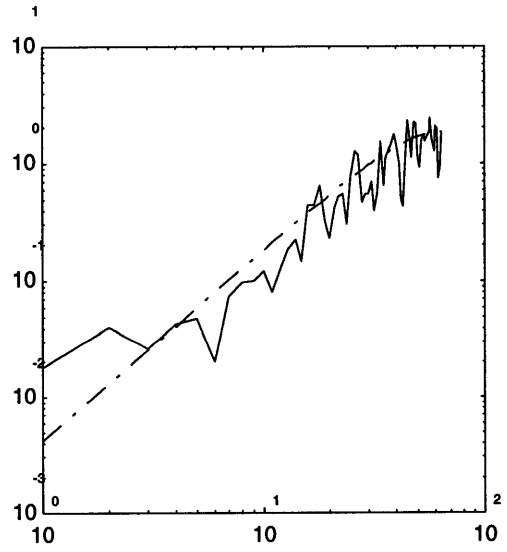

Figure 24: Power spectrum of the reflectivity series of the Ste. Helene well. The dotted line shows the power spectrum of the best-fitting fractionally integrated noise process.

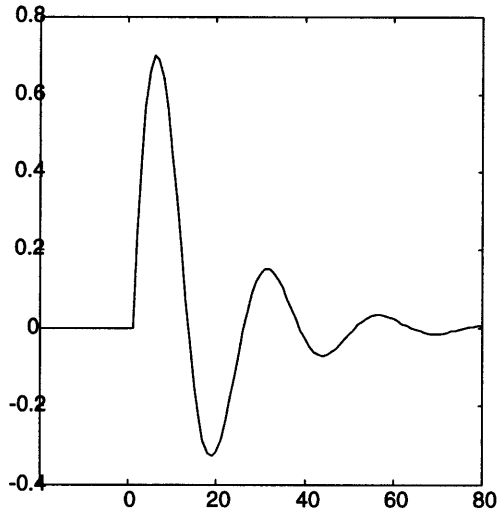

Figure 25: Source wavelet used to calculate the synthetic traces.

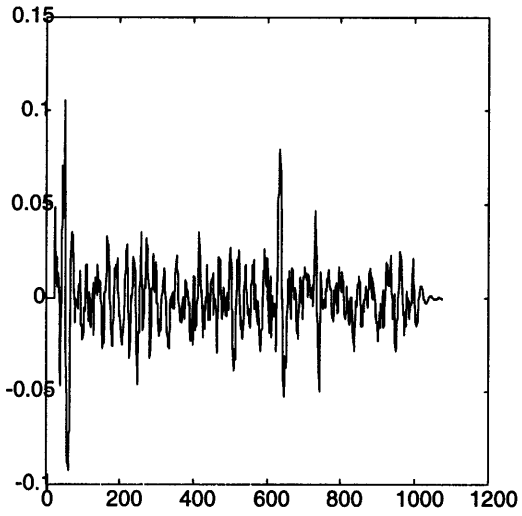

Figure 26: Synthetic trace derived from the reflectivity series of the Ste. Helene well.

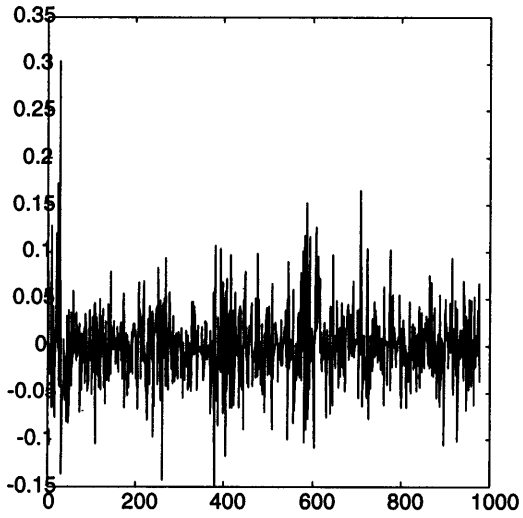

Figure 27: Recovered reflectivity series for the Ste. Helene well using conventional deconvolution.

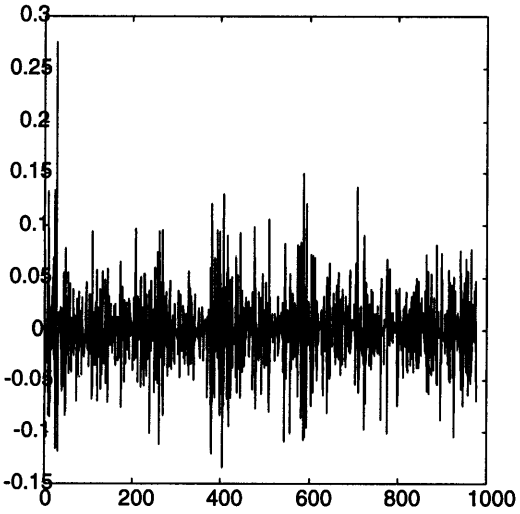

Figure 28: Recovered reflectivity series for the Ste. Helene well using generalized deconvolution. Here, d is taken to be -0.82.

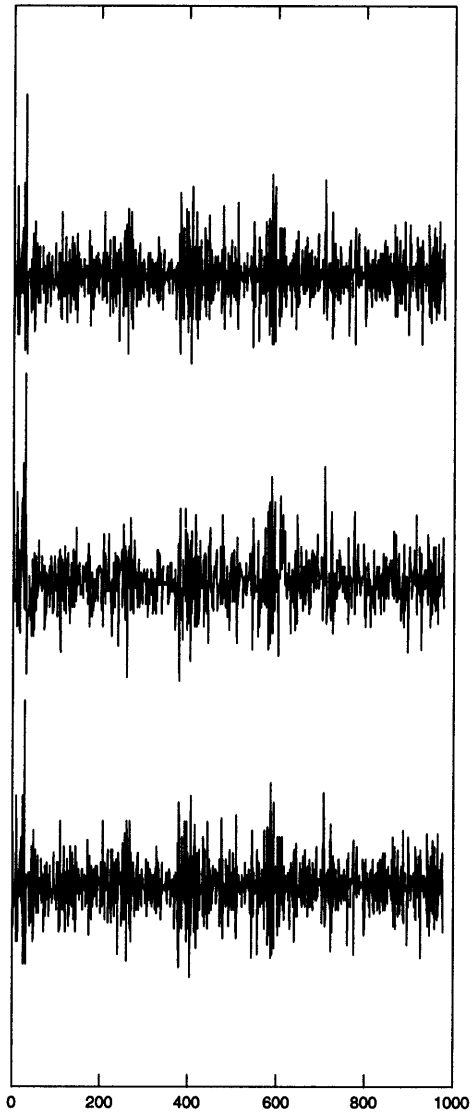

Figure 29: The top graph shows the real reflectivity series for the Ste. Helene well. The bottom two graphs show those produced by the conventional and generalized deconvolution filters, respectively.

Performance Evaluation

Two methods of comparison are used to evaluate the performance of the generalized deconvolution based on fractionally integrated noise. The first is the residual wavelet. Here we compute the residual wavelet remaining in the output trace after deconvolution (Jurkevics and Wiggins, 1984) by dividing the output trace by the true reflectivity series in the frequency domain and transforming the result to the time domain. For perfect deconvolution, the residual wavelet should be a spike. The deviation from a spike is then a measure of the performance of the deconvolution filter.

The second method is based on the RMS (*root-mean-square*) error between the recovered reflectivity series $\{r_t\}$ (the output of the deconvolution filter) and the exact series $\{e_t\}$. The RMS error is defined by

$$\text{RMS error} = \sqrt{\frac{\sum_t (e_t - r_t)^2}{\sum_t e_t^2}} \tag{16}$$

Performance Analysis – Example 1

Figures 27 and 28 show the recovered reflectivity series after performing the conventional and generalized Wiener deconvolutions, respectively, on the synthetic trace. The order of the fractionally integrated noise process used here is that corresponding to the best-fitting power spectrum, -0.82 in this case. The advantage of generalized deconvolution is evident here: its output, contrary to that of conventional deconvolution, is indistinguishable by eye from the true reflectivity series. Figure 29 combines figures 23, 27 and 28 in a single graph to make the comparison between the outputs of the two filters easier.

Figures 30 and 31 show the residual wavelets left by conventional and generalized deconvolutions, respectively. Again, the advantage of the generalized scheme is apparent: its residual wavelet is much more spike-like than that of the conventional scheme.

Sensitivity to the Order of the Underlying Process

Figures 32 through 36 show the residual wavelets left by generalized deconvolution where the order of the fractionally integrated noise process is assumed to be -0.2, -0.4, -0.6, -0.8 and -1.0, respectively. This is computed to test the sensitivity of generalized deconvolution to the order of the fractionally integrated noise process assumed to represent the reflectivity series. As can be seen in the figures, generalized deconvolution seems to outperform the conventional one regardless of the assumed order of the process, so long as it is chosen within a reasonable interval (typically between -1 and zero). Figure 37 combines figures 30 to 36 in a single graph to make the comparison easier.

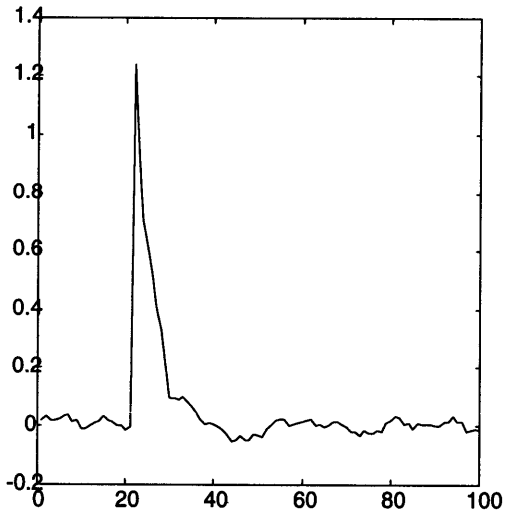

Figure 30: Residual wavelet left by conventional deconvolution for the Ste. Helene well.

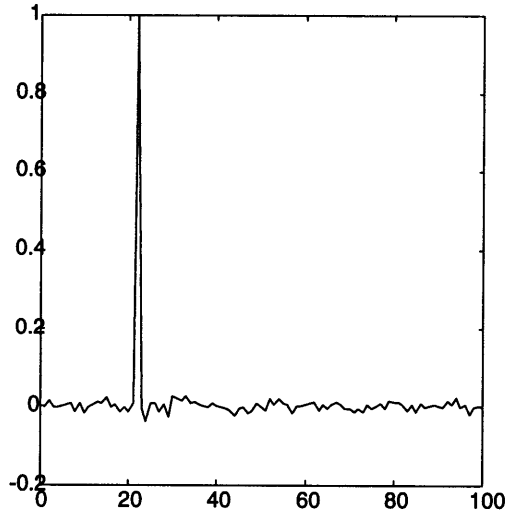

Figure 31: Residual wavelet left by generalized deconvolution for the Ste. Helene well. Here, d is taken to be -0.82.

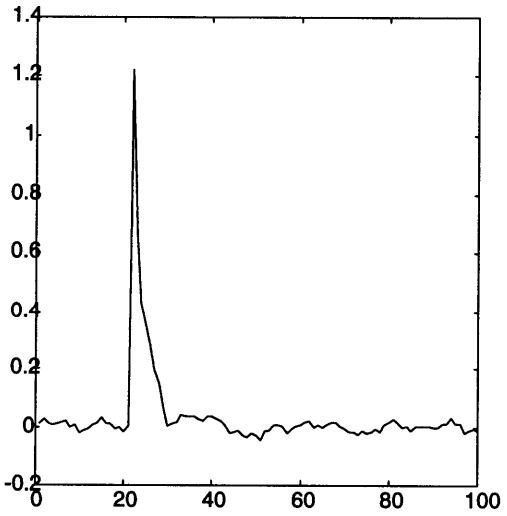

Figure 32: Residual wavelet left by generalized deconvolution for the Ste. Helene well. Here, d is taken to be -0.2.

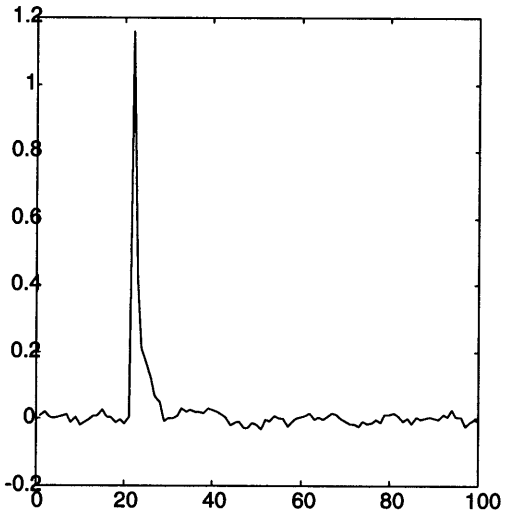

Figure 33: Residual wavelet left by generalized deconvolution for the Ste. Helene well. Here, d is taken to be -0.4.

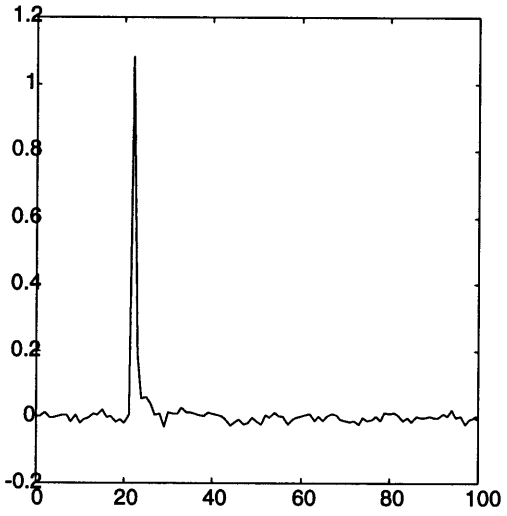

Figure 34: Residual wavelet left by generalized deconvolution for the Ste. Helene well. Here, d is taken to be -0.6.

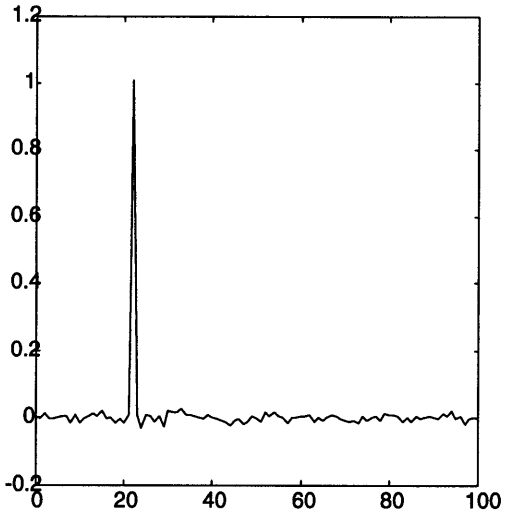

Figure 35: Residual wavelet left by generalized deconvolution for the Ste. Helene well. Here, d is taken to be -0.8.

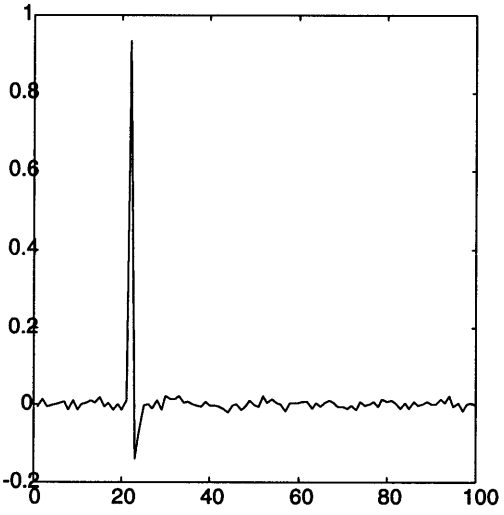

Figure 36: Residual wavelet left by generalized deconvolution for the Ste. Helene well. Here, d is taken to be -1.0.

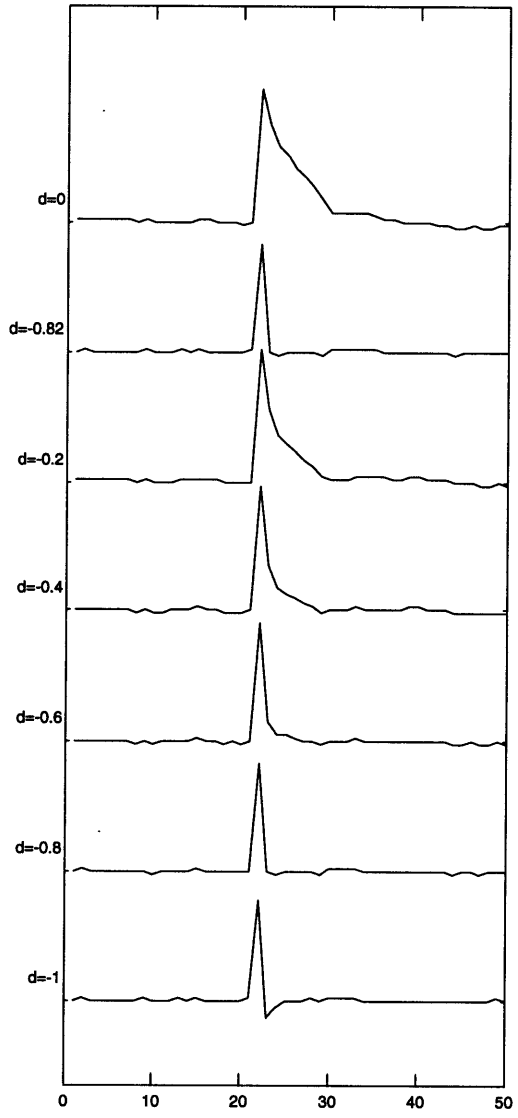

Figure 37: From top: Residual wavelet left by conventional deconvolution (top) and generalized deconvolution where d is taken to be -0.82 (best-fitting), -0.2, -0.4, -0.6, -0.8, and -1, respectively. All for the Ste. Helene well.

Finally, figure 38 shows the percentage RMS error associated with generalized deconvolution as a function of the order of the fractionally integrated noise process assumed to represent the true reflectivity series. Again, this is a test of the sensitivity of generalized deconvolution to this parameter. The case of $d = 0$ represents conventional deconvolution. It is evident here as well that generalized deconvolution outperforms the conventional one in almost all reasonable choices of the parameter d, signifying that an accurate knowledge of the correlation structure of the reflection coefficients is not necessary for this deconvolution scheme to work.

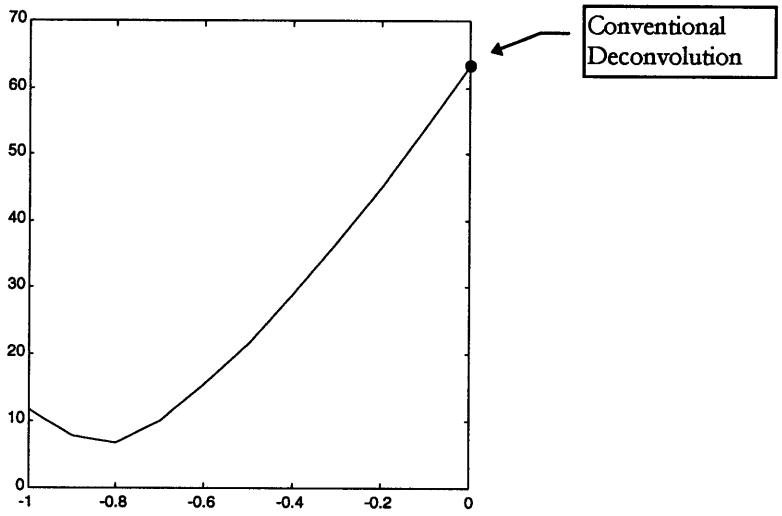

Figure 38: Percentage RMS error for generalized deconvolution as a function of the order of the fractionally integrated noise process taken to represent the reflectivity series of the Ste. Helene well. Note that d = 0 corresponds to conventional deconvolution.

Performance Analysis – Example 2

The analysis for the Wickham well follows the same manner as that for the Ste. Helene well, and the results obtained from it corroborate those derived above. Figure 39 shows the reflection coefficients of the Wickham well. Figure 40 shows the power spectrums of that reflectivity series and the best-fitting fractionally integrated noise process (denoted by the dotted line), which was found to be -0.70 in this case. We use the same wavelet as before (figure 25), together with the reflectivity series of this well to produce a synthetic trace, shown on figure 41. Figures 42 and 43 show the recovered reflectivity series after performing the conventional and generalized deconvolutions, respectively, on the synthetic trace. Like before, the output of generalized deconvolution filter is indistinguishable by eye from the true reflectivity series, unlike that of conventional deconvolution (figure 44 combines figures 39, 42 and 43 in a single graph to make the comparison easier).

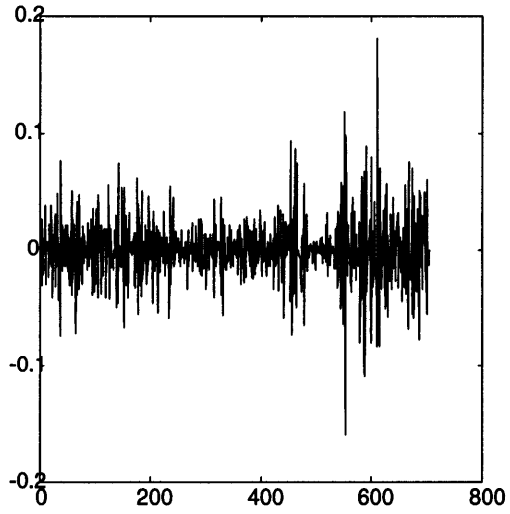

Figure 39: Reflection coefficients of the Wickham well.

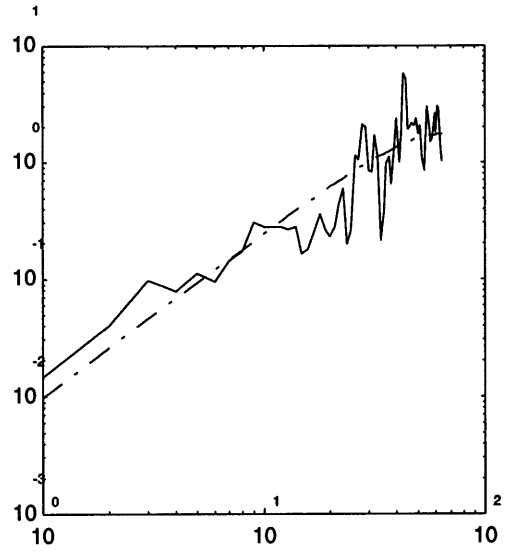

Figure 40: Power spectrum of the reflectivity series of the Wickham well. The dotted line shows the power spectrum of the best-fitting fractionally integrated noise process.

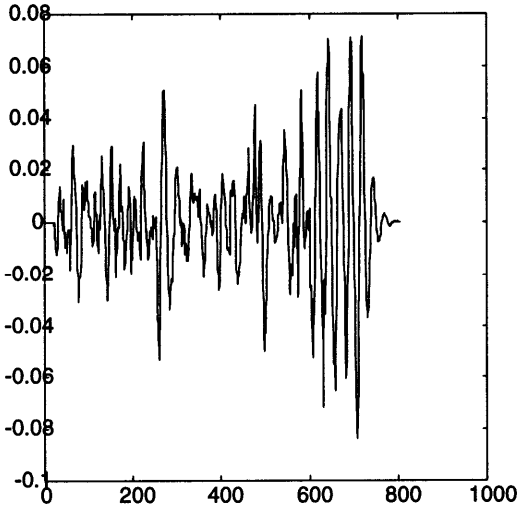

Figure 41: Synthetic trace derived from the reflectivity series of the Wickham well.

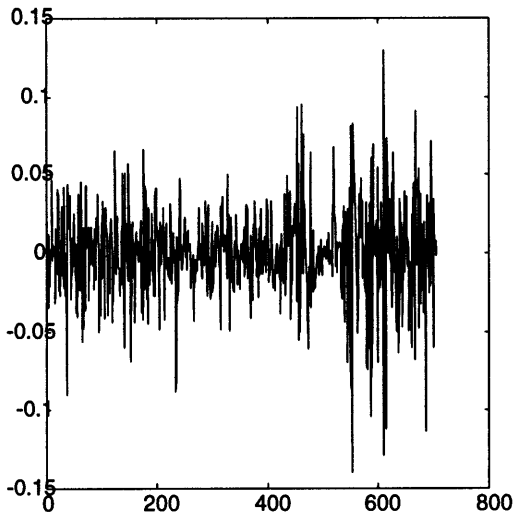

Figure 42: Recovered reflectivity series for the Wickham well using conventional deconvolution.

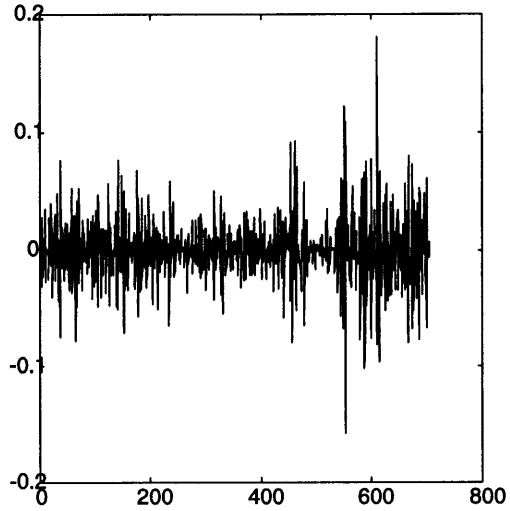

Figure 43: Recovered reflectivity series for the Wickham well using generalized deconvolution. Here, d is taken to be -0.70.

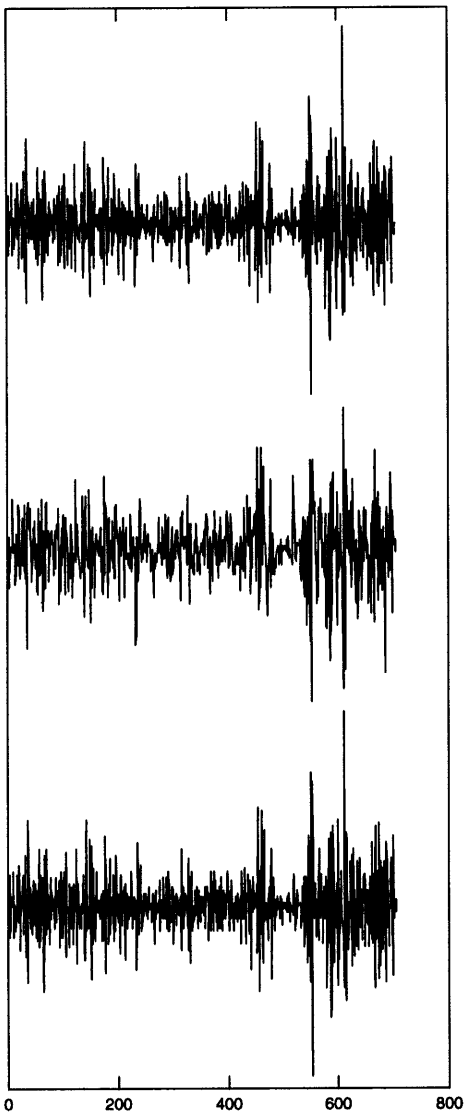

Figure 44: The top graph shows the real reflectivity series for the Wickham well. The bottom two graphs show those produced by the conventional and generalized deconvolution filters, respectively.

Figures 45 through 51 show, respectively, the residual wavelet left by conventional deconvolution and those left by generalized deconvolution using orders of -0.70 (best-fitting fractionally integrated noise process), -0.2, -0.4, -0.6, -0.8 and -1.0 (figure 52 combines these in a single graph to make the comparison easier). We make the same observation here like before that generalized deconvolution seems to outperform the conventional one regardless of the assumed order of the process over the (-1, 0) interval.

Finally, figure 38 shows the percentage RMS error associated with generalized deconvolution as a function of the order of the fractionally integrated noise process. A similar conclusion to the above can be drawn here as well.

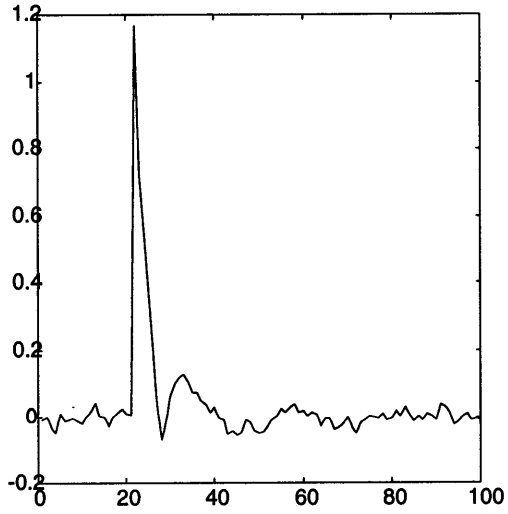

Figure 45: Residual wavelet left by conventional deconvolution for the Wickham well.

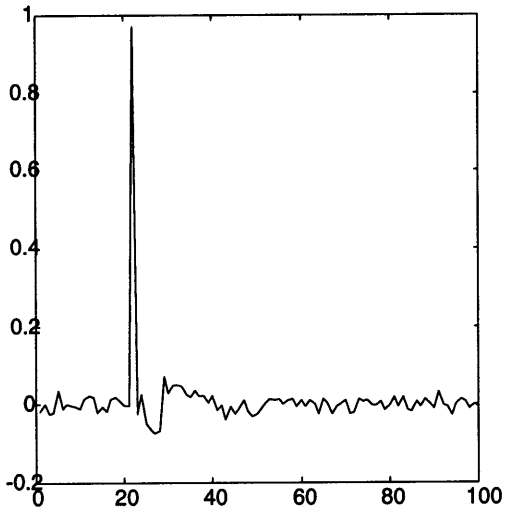

Figure 46: Residual wavelet left by generalized deconvolution for the Wickham well. Here, d is taken to be -0.70.

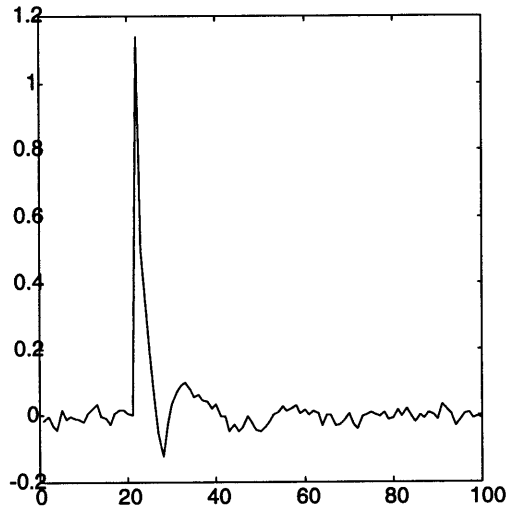

Figure 47: Residual wavelet left by generalized deconvolution for the Wickham well. Here, d is taken to be -0.2.

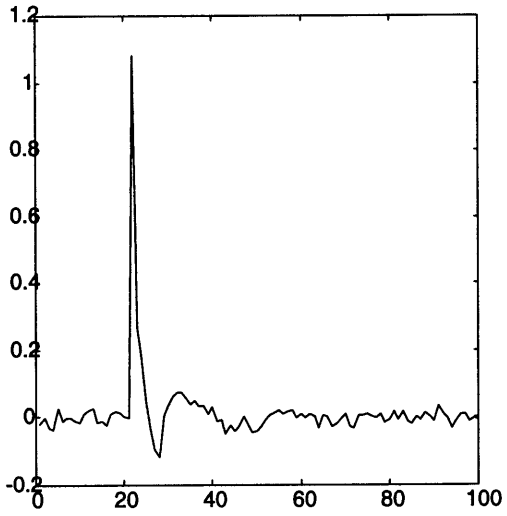

Figure 48: Residual wavelet left by generalized deconvolution for the Wickham well. Here, d is taken to be -0.4.

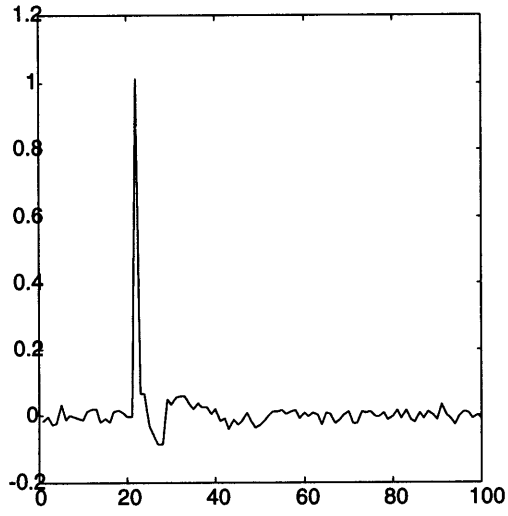

Figure 49: Residual wavelet left by generalized deconvolution for the Wickham well. Here, d is taken to be -0.6.

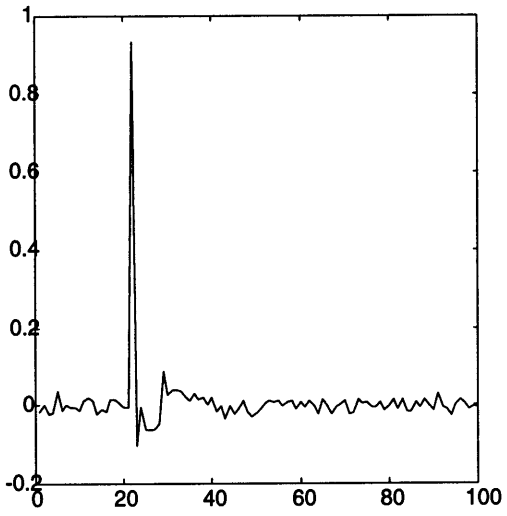

Figure 50: Residual wavelet left by generalized deconvolution for the Wickham well. Here, d is taken to be -0.8.

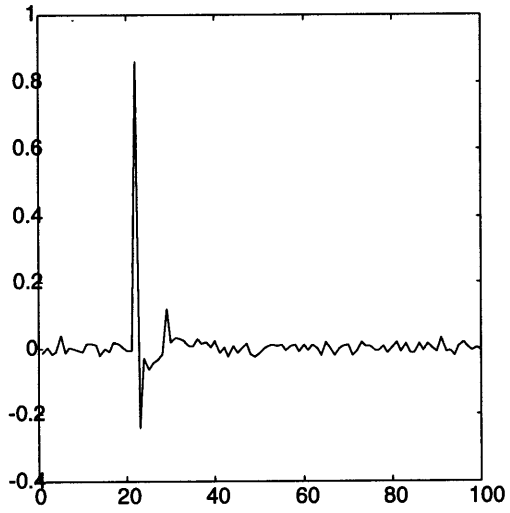

Figure 51: Residual wavelet left by generalized deconvolution for the Wickham well. Here, d is taken to be -1.0.

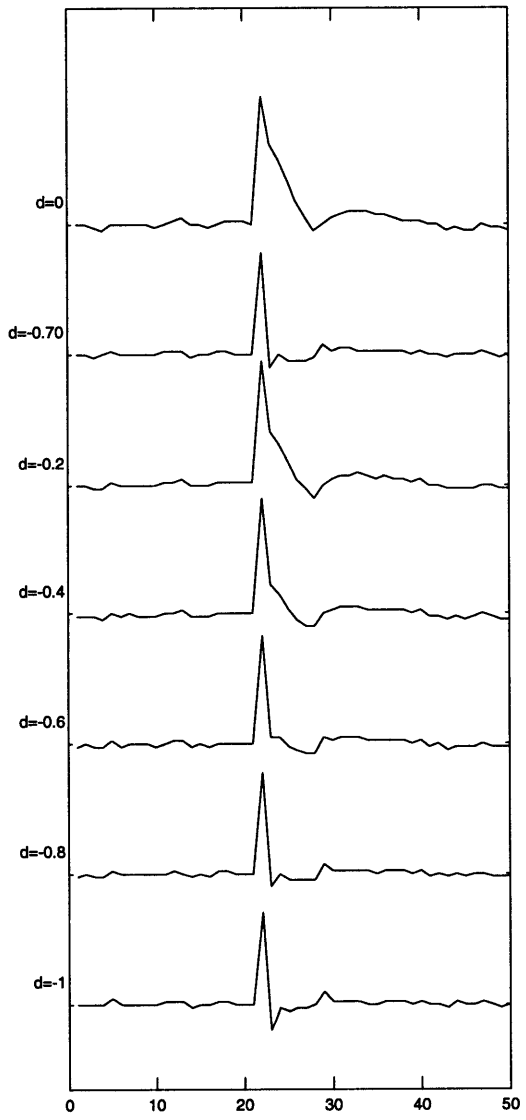

Figure 52: From top: Residual wavelet left by conventional deconvolution (top) and generalized deconvolution where d is taken to be -0.70 (best-fitting), -0.2, -0.4, -0.6, -0.8, and -1, respectively. All for the Wickham well.

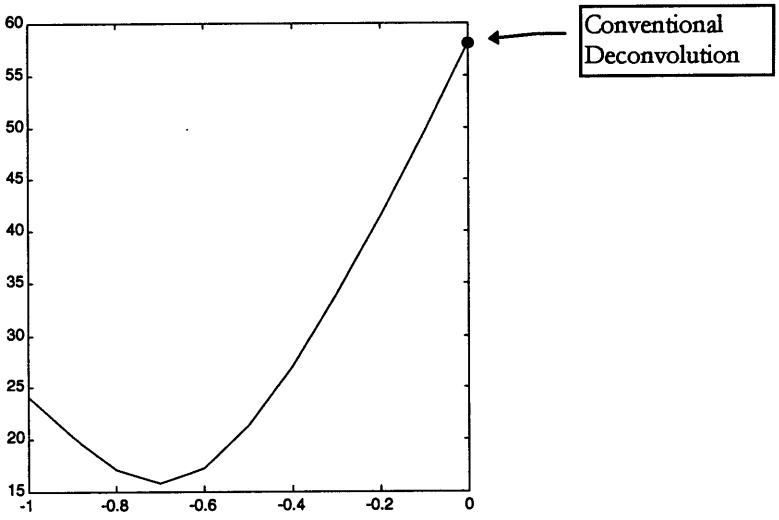

Figure 53: Percentage RMS error for generalized deconvolution as a function of the order of the fractionally integrated noise process taken to represent the reflectivity series of the Wickham well. Note that d = 0 corresponds to conventional deconvolution.

SUMMARY AND CONCLUSIONS

The purpose of this thesis was to generalize the conventional Weiner deconvolution method to take into account the non-white-noise behavior of the earth's reflection coefficients, since they are observed in nature to have power spectra that are proportional to frequency rather than independent of it as a white noise model would suggest.

To achieve that, we introduced the fractionally integrated noise process, whose stochastic properties approximate those observed of reflectivity to a much greater extent than random white noise. We then gave an efficient implementation to compute the modified deconvolution filter based on this process. The new procedure is a generalization of the conventional one in that it reduces to the latter when the underlying fractionally integrated noise process becomes white noise. We analyzed the computational requirements of the proposed implementation and found it to need about an order of magnitude less calculations than the method suggested by Todoeschuck and Jensen (1988).

The effectiveness of the generalized filter was studied by applying it to synthetic traces derived from real well log data. We compared the outputs of both the generalized and conventional deconvolution filters to the exact reflection coefficients used to produce the traces. Two methods of comparison were used: the residual wavelet left in the trace after applying the filter and the RMS error between the output of the filter and the exact series.

In both of the wells used to make the analysis, the generalized filter seems to consistently outperform the conventional one over a wide range of the

choice of the underlying fractionally integrated noise process parameter, indicating that even a poor choice of the parameter would still yield favorable results. With this and the above in mind, we would like to recommend the adoption and use of the generalized filter, especially in areas where the reflection coefficients are observed from nearby wells logs to deviate significantly from the white noise model. In these cases, the data from the well logs can also aid in the choice of the fractionally integrated noise parameter used to calculate the generalized filter.

REFERENCES

Barrodale, I. and Roberts, F. D. K., An improved algorithm for discrete l_1 linear approximation, *SIAM J. Num. Anal.*, **10**:839, 1973.

Beyer, William H., *CRC Standard Mathematical Tables*, CRC Press, Boca Raton, 1987.

Box, George E. and Jenkins, Gwilym M., *Time Series Analysis: Forecasting and Control*, Holden-Day, Oakland, California, 1976.

Brockwell, Peter J. and Davis, Richard A., *Time Series: Theory and Methods*, Springer-Verlag, New York, 1987.

Burg, J. P., *Maximum entropy spectral analysis*, Stanford University, 1975. Ph.D. thesis.

Buttkus, B., Homomorphic filtering - theory and practice, *Geophysical Prospecting*, **23**:712-748, 1975.

Claerbout, J. F., *Fundamentals of Geophysical Data Processing*, McGraw-Hill, 1976.

Clarke, G. K. C., Time-varying deconvolution filters, *Geophysics*, **33**:936-944, 1968.

Crump, Norman D., A Kalman filter approach to the deconvolution of seismic signals, *Geophysics*, **39**:1-13, 1974.

Griffiths, L. J., Smolka, F. R. and Trembly, L. D., Adaptive deconvolution: A new technique for processing time-varying seismic data, *Geophysics*, **42**:742-759, 1977.

Hosken, J. W. J., A stochastic model for seismic reflections, In *50th Annual Meeting Abstracts*, Society of Exploration Geophysics, Houston, 1980. (Abstract G-69, Geophysics 46, 419).

Hosking, J. R. M., Fractional differencing, *Biometrika*, **68**:165-176, 1981.

Hosking, J. R. M., Modeling persistence in hydrological time series using fractional differencing, *Water Resources Research*, **20**:1898-1908, 1984.

Jurkevics, Andrejs and Wiggins, Ralphe, A critique of seismic deconvolution methods, *Geophysics*, **49**:2109-2116, 1984.

Mandelbrot, B. B., *The Fractal Geometry of Nature*, W. H. Freeman and Co., New York, 1983.

Mendel, Jerry M., *Optimal Seismic Deconvolution*, Academic Press, New York, 1983.

Ott, N. and Meder, H. G., The Kalman filter as a prediction error filter, *Geophysical Prospecting*, **20**:549-560, 1972.

Peacock, K. L. and Treitel, Sven, Predictive deconvolution: Theory and practice, *Geophysics*, **34**:155-169, 1968.

Pilkington, M. and Todoeschuck, J. P., Stochastic inversion for scaling geology, *Geophysical Journal International*, **102**:205-217, 1990.

Press, William H, Flannery, Brian P., Teukolsky, Saul A. and Vetterling, William T., *Numerical Recipes in C*, Cambridge University Press, Cambridge, 1988.

Priestley, M. B., *Spectral Analysis and Time Series*, Academic Press, London, 1981.

Ramsey, F. L., Characterization of the partial autocorrelation function, *Ann. Stat.*, **2**:1296-1301, 1974.

Robinson, Enders A. and Treitel, Sven, *Geophysical Signal Analysis*, Prentice-Hall, Englewood Cliffs, NJ, 1980.

Rosa, A. L. R. and Ulrych, T. J., Processing via spectral modeling, *Geophysics*, **56**:1244-1251, 1991.

Shtatland, E. S., Fractal stochastic models for acoustic impedance, an explanation of scaling or 1/f geology, and stochastic inversion, In *Expanded Abstracts of the 61st Annual International SEG Meeting*, SEG, Houston, Nov. 10-14, 1991.

Shtatland, E. S. and Toksöz, M. N., On fractal modeling for acoustic impedance and an explanation of scaling or 1/f geology, *EOS, Transactions of the American Geophysical Union*, **72**:59, 1991.

Todoeschuck, John P. and Jensen, Oliver G., Joseph geology and seismic deconvolution, *Geophysics*, **53**:1410-1414, 1988.

Todoeschuck, J. P., Jensen, O. G. and Labonte, S., Gaussian scaling noise model of seismic reflection sequences: Evidence from well logs, *Geophysics*, **55**:480-484, 1990.

Vanmarcke, E., *Random Fields: Analysis and Synthesis*,, MIT Press, Cambridge, 1989.

Walden, A. T. and Hosken, J. W. J., An investigation of the spectral properties of primary reflection coefficients, *Geophysical Prospecting*, **33**:400-435, 1985.

Wiggins, Ralphe, Minimum entropy deconvolution, *Geoexploration*, **16**:21-35, 1978.

Wiggins, Ralphe, Entropy guided deconvolution, *Geophysics*, **50**:2720-2726, 1985.

Ulrych, T. J., Application of homomorphic deconvolution to seismiology, *Geophysics*, **36**:650-660, 1971.

Yilmaz, Özdogan, *Seismic data Processing*, Society of Exploration Geophysics, Tulsa, Oklahoma, 1987.

Ziolkowski, A. M., *Deconvolution*, IHRDC Publishers, 1984.

Ziolkowski, Anton and Slob, Evert, Can we perform statistical deconvolution by polynomial factorization?, *Geophysics*, **56**:1423-1431, 1991.

APPENDIX A: SYNTHESIZING FRACTIONALLY INTEGRATED NOISE SAMPLES

We discuss here a method of producing synthetic samples of a fractionally integrated noise process of a given order. We first note that any Gaussian stationary stochastic process is completely characterized by its mean, variance, and auto-correlation function (Box and Jenkins, 1976). Thus, producing a synthetic realization of a Gaussian fractionally integrated noise process of order d that has zero mean and variance γ_0 is equivalent to producing a realization of a Gaussian process of such mean and variance that has an auto-correlation function given by equation (2). The reader is reminded here again of the difference between the correlation structure of the process (i.e. being a fractionally integrated noise process) and the probability distribution structure (i.e. being Gaussian).

Next, we note that for any stationary linear stochastic process $\{y_t\}$ of zero mean, the conditional mean and variance given the past values $y_{t-1}, y_{t-2}, \ldots, y_0$ is described by (Ramsey, 1974; Hosking, 1984)

$$E(y_t \mid y_{t-1}, y_{t-2}, \ldots, y_0) = \sum_{j=1}^{t} \phi_{tj}\, y_{t-j} \tag{17}$$

$$V(y_t \mid y_{t-1}, y_{t-2}, \ldots, y_0) = \gamma_0 \prod_{j=1}^{t} (1 - \phi_{jj}^2) \tag{18}$$

which we can write as

$$\mu_t = \sum_{j=1}^{t} \phi_{tj}\, y_{t-j} \tag{19}$$

$$v_t = \gamma_0 \prod_{j=1}^{t} (1 - \phi_{jj}^2) \tag{20}$$

In the above equations, γ_0 is the (unconditional) variance of $\{y_t\}$, ϕ_{jj} is the jth partial correlation coefficient, and ϕ_{ij} are the partial linear regression coefficients. Those coefficients can be found using the Durbin recursive formula

$$\phi_{ij} = \phi_{t-1,j} - \phi_{tt}\phi_{t-1,j-1} \qquad j = 1,\ldots,t-1 \tag{21}$$

Equation (20) can be written as

$$v_t = (1 - \phi_{tt}^2) v_{t-1} \tag{22}$$

Finally, the kth partial correlation coefficient of a fractionally integrated noise process of order d is given by

$$\phi_{kk} = \frac{d}{1-d} \tag{23}$$

From (19) and (20) we see that to produce a sample $y_0, y_1, \ldots, y_n$ of a process that has zero mean, variance γ_0, and auto-correlation function ρ_k, we must generate each random number y_t from a Gaussian distribution of mean μ_t and variance v_t. Hence, the sample would be

$$\{y_0, y_1, \ldots, y_n\}$$
where
$$y_t \in G(\mu_t, v_t) \tag{24}$$

The problem is thus reduced to calculating μ_t and v_t for $t = 0,1,\ldots,N$. Once these are found, a random number is generated from the corresponding Gaussian distribution at each stage.

We can therefore now give a recursive procedure for synthesizing a realization of a fractionally integrated noise process of order d that has zero mean and a variance of γ_0:

1. Generate a starting random value y_0 from a Gaussian distribution of zero mean and variance $\upsilon_0 = \gamma_0$. In other words, $y_0 \in G(0,\gamma_0)$.
2. For $t = 1,2,\ldots,n$, calculate ϕ_{tt} from (21) and the previous values found by this recursion.
3. Calculate μ_t and υ_t from (19) and (22) using the values found in the previous step and earlier iterations.
4. Repeat steps 2 and 3 to generate the entire sample.

The computer code (written in the C language) that implements the above procedure and that was used to synthesize the samples in this thesis is included below.

```
/*
 * Generates a fractionally integrated
 * noise sample of length n. The sample
 * is normally distributed with zero
 * mean and unit variance
 */

/*
 * The program uses the Numerical Recipes
 * library. In particular, it uses the
 * function gasdev(), which returns a
 * normally distributed deviate with zero
 * mean and unit variance (Press et al., 1988).
 */

/*
 * The program takes three arguments: the
 * length of the sample, the order of the
 * process and the output file name.
 */
```

```
/*
 * Standard include files.
 */

#include "stdio.h"
#include "math.h"

/*
 * This is the header for the Numerical
 * Recipes library.
 */

#include "nr.h"

/*
 * Maximum length of the sample
 */

#define MAX 1000

/*
 * Main (and only) function.
 */

void main(int argc, char *argv[])
{

/*
 * fo   output file handle
 * fn   output file name
 * n    length of the sample
 * d    order of the process
 * x    the sample
 * var  variance
 */

FILE *fo;
char *fn;
int n, t, j, *idum;

float x[MAX], phi[MAX][MAX], d, var, mean;

/*
 * Make sure we have enough arguments
 */

if(argc<4) {
  printf("usage: %s n d file\n", argv[0]);
```

```
  exit(0);
}

/*
 * Convert the arguments to numbers
 */

n = atoi(argv[1]);
d = atof(argv[2]);
fn = argv[3];

t = 1;
idum = &t;

/*
 * Initialize the recursive iterations
 */

var = 1;
x[0] = gasdev(idum);

/*
 * Main recursive loop. It is recursive
 * mathematical-wise, not computer-wise.
 */

for(t=1; t<=n-1; t++) {

  phi[t][t] = d/(t-d);

  for(j=1; j<=t-1; j++)
    phi[t][j] = phi[t-1][j]-phi[t][t]*phi[t-1][t-j];

  mean = 0;
  for(j=1; j<=t; j++)
    mean = mean+phi[t][j]*x[t-j];

  var = var*(1-phi[t][t]*phi[t][t]);
  x[t] = sqrt(var)*gasdev(idum) + mean;

  }

/*
 * Write the result to the output file.
 */

fo = fopen(fn, "w");
for(j=0; j<=n-1; j++)
```

```
  fprintf(fo, "%f\r\n", x[j]);
fclose(fo);

}

/*
 * End.
 */
```

APPENDIX B: PROCESS PARAMETER ESTIMATION

We would like here to find the order of the fractionally integrated noise process whose power spectrum gives the best approximation to that of the data. In other words, we want to fit the power spectrum of the data by that of a fractionally integrated noise of order d such that the difference between the two is minimal.

Let's denote the order of the fractionally integrated noise process in this appendix by q instead of d to avoid any confusion with the differentiation symbol in the equations that follow. From (3) we have

$$P_q(f) = \sqrt{\pi}\frac{\Gamma(1-q)}{\Gamma(\frac{1}{2}-q)}\sin^{-2q}(\pi f) \tag{25}$$

(with no loss of generality we have assumed here that $\sigma^2 = 1$). Denote the power spectrum of the reflections coefficients derived from the well log data by y_i for $i = 0,1,\ldots,N$, where N is the number of observations in the data. The Error between the calculated power spectrum and the actual one is thus given by

$$e_i = P_q(f_i) - y_i \qquad i = 0,1,\ldots,N \tag{26}$$

We would like to find the order q that minimizes this error in the least-squares sense. Hence, we want to minimize the expression

$$\begin{aligned} |E|^2 &= \sum_{i=0}^{N} e_i^2 \\ &= \sum_{i=0}^{N}\left(P_q(f_i) - y_i\right)^2 \end{aligned} \tag{27}$$

with respect to the parameter q.

To simplify the derivation we first show that given any differentiable function $f(x)$ and a strictly monotonically increasing function $g(x)$, the composite function $g \circ f$ has its local minima at exactly the points that f has its minima. In other words, if $g \circ f$ has a local minimum at x_m, then f must have a local minimum at x_m.

Suppose that $g \circ f$ has a local minimum at x_m, then

$$\frac{d}{dx}(g \circ f)(x_m) = 0 \tag{28}$$

and

$$\frac{d^2}{dx^2}(g \circ f)(x_m) > 0 \tag{29}$$

Now

$$\frac{d}{dx}(g \circ f)(x) = \frac{d}{dx} g(f(x)) \cdot \frac{d}{dx} f(x) \tag{30}$$

Hence, from (28) we have

$$\frac{d}{dx} g(f(x_m)) \cdot \frac{d}{dx} f(x_m) = 0 \tag{31}$$

However, since g is a monotonic function, it has no local extrema, and thus

$$\frac{d}{dy} g(y) \neq 0 \qquad \text{for all } y \tag{32}$$

From (31) and (32) we get

$$\frac{d}{dx} f(x_m) = 0 \tag{33}$$

Moreover,

$$\begin{aligned} \frac{d^2}{dx^2}(g \circ f)(x) &= \frac{d}{dx}\left[\frac{d}{dx}(g \circ f)(x)\right] \\ &= \frac{d}{dx}\left[\frac{d}{dx} g(f(x)) \cdot \frac{d}{dx} f(x)\right] \\ &= \frac{d^2}{dx^2} g(f(x)) \cdot \left(\frac{d}{dx} f(x)\right)^2 \\ &\quad + \frac{d}{dx} g(f(x)) \cdot \frac{d^2}{dx^2} f(x) \end{aligned} \tag{34}$$

So, at x_m we have (using (33))

$$\begin{aligned} \frac{d^2}{dx^2}(g \circ f)(x_m) &= \frac{d^2}{dx^2} g(f(x_m)) \cdot \left(\frac{d}{dx} f(x_m)\right)^2 \\ &\quad + \frac{d}{dx} g(f(x_m)) \cdot \frac{d^2}{dx^2} f(x_m) \\ &= 0 + \frac{d}{dx} g(f(x_m)) \cdot \frac{d^2}{dx^2} f(x_m) \end{aligned} \tag{35}$$

From that and (29) we get

$$\frac{d}{dx} g(f(x_m)) \cdot \frac{d^2}{dx^2} f(x_m) > 0 \tag{36}$$

However, since g is a strictly increasing function, we have

$$\frac{d}{dy} g(y) > 0 \qquad \text{for all } y \tag{37}$$

Thus, from (36) and (37), we have

$$\frac{d^2}{dx^2} f(x_m) > 0 \tag{38}$$

Equations (33) and (38) show that f has a local minimum at x_m, as suggested.

With the above in mind, let's set $g(x) = \ln(x)$ and take the logarithm of both sides of equation (25). We get

$$\ln P_q(f_i) = \tfrac{1}{2}\ln\pi + \ln\Gamma(1-q) - \ln\Gamma(\tfrac{1}{2}-q) - 2q\ln\sin(\pi f_i) \tag{39}$$

Now let

$$\begin{aligned} a &= \tfrac{1}{2}\ln\pi \\ h(q) &= \ln\Gamma(1-q) - \ln\Gamma(\tfrac{1}{2}-q) \\ x_i &= -2\ln\sin(\pi f_i) \\ z_i &= \ln y_i \end{aligned} \tag{40}$$

Equation (39) then becomes

$$\ln P_q(f_i) = a + h(q) + qx_i \tag{41}$$

Therefore, in order to minimize (27), we can just minimize the expression

$$\begin{aligned} \left|\hat{E}\right|^2 &= \sum_{i=0}^{N} \left(\ln P_q(f_i) - \ln y_i\right)^2 \\ &= \sum_{i=0}^{N} \left(a + h(q) + qx_i - z_i\right)^2 \end{aligned} \tag{42}$$

To minimize (42), we set the derivative with respect to q to zero. Hence, we have

$$
\begin{aligned}
0 &= 2\sum_{i=0}^{N}\left(a+h(q)+qx_i-z_i\right)\left(\frac{dh}{dq}+x_i\right) \\
&= \sum_{i=0}^{N}\left(a\frac{dh}{dq}+ax_i+h\frac{dh}{dq}+hx_i+q\frac{dh}{dq}x_i+qx_i^2-z_i\frac{dh}{dq}-x_iz_i\right) \\
&= N\frac{dh}{dq}(a+h)+\left(a+h+q\frac{dh}{dq}\right)\sum_{i=0}^{N}x_i+q\sum_{i=0}^{N}x_i^2-\frac{dh}{dq}\sum_{i=0}^{N}z_i-\sum_{i=0}^{N}x_iz_i
\end{aligned}
\tag{43}
$$

So

$$
N\frac{dh}{dq}(a+h)+\left(a+h+q\frac{dh}{dq}\right)\sum_{i=0}^{N}x_i+q\sum_{i=0}^{N}x_i^2-\frac{dh}{dq}\sum_{i=0}^{N}z_i-\sum_{i=0}^{N}x_iz_i=0 \tag{46}
$$

Hence, the fractionally integrated noise order q that gives the best fit is found by solving (46). This can be done numerically. Note that except for $\frac{dh}{dq}$, the terms in (46) are easily calculable from (40). Let's write $\frac{dh}{dq}$ in a form that would make it easier to compute.

$$
\begin{aligned}
\frac{dh}{dq} &= \frac{d}{dq}\left[\ln\Gamma(1-q)-\ln\Gamma(\tfrac{1}{2}-q)\right] \\
&= \frac{\Gamma'(1-q)}{\Gamma(1-q)}\cdot(-1)-\frac{\Gamma'(\frac{1}{2}-q)}{\Gamma(\frac{1}{2}-q)}\cdot(-1) \\
&= \frac{\Gamma'(\frac{1}{2}-q)}{\Gamma(\frac{1}{2}-q)}-\frac{\Gamma'(1-q)}{\Gamma(1-q)} \\
&= \Psi(\tfrac{1}{2}-q)-\Psi(1-q)
\end{aligned}
\tag{47}
$$

where

$$\Psi(x) = \frac{\Gamma'(x)}{\Gamma(x)} = -\gamma + \sum_{n=0}^{\infty}\left(\frac{1}{n+1} - \frac{1}{x+n}\right) \tag{48}$$

(Beyer, 1987). γ is called Euler's constant, and its value is approximately given by

$$\gamma = 0.5772157\ldots \tag{49}$$

The function Ψ can thus be computed numerically from (48) up to a suitable cut-off upper limit as dictated by the desired accuracy when solving (43) in the computer.

APPENDIX C: CALCULATING GENERALIZED DECONVOLUTION

Suppose that for a given input $\{x_t\}$ we would like to design a filter f such that the output is $\{y_t\}$. We'll therefore call $\{y_t\}$ the desired output. Applying the filter on the input, we get

$$f * x = \hat{y} \tag{50}$$

where $\{\hat{y}_t\}$ is the actual output, which we want to be a good an approximation of the desired output.. The filter that gives rise to the best approximation of the desired output is the one that minimizes the difference between the desired and actual outputs. Hence would like to find the filter $f = (f_0, f_1, \ldots, f_m)$ that minimizes the difference (Robinson and Treitel, 1980)

$$L = E\left\{(y_t - \hat{y}_t)^2\right\} \tag{51}$$

which is the expected value of the least-squares distance between the two.

From (50), (51) and the definition of convolution we gave earlier, we have

$$L = E\left\{\left(y_t - \sum_{k=0}^{m} f_k x_{t-k}\right)^2\right\} \tag{52}$$

To minimize this in terms of the coefficients of the filter, we set the partial derivative with respect to each of the coefficients to zero. Therefore, we have for $j = 0,1,\ldots,m$

$$
\begin{aligned}
0 &= \frac{\partial}{\partial f_j} E\left\{\left(y_t - \sum_{k=0}^{m} f_k x_{t-k}\right)^2\right\} \\
&= E\left\{2\left(y_t - \sum_{k=0}^{m} f_k x_{t-k}\right)\frac{\partial}{\partial f_j}\left(y_t - \sum_{k=0}^{m} f_k x_{t-k}\right)\right\} \\
&= 2E\left\{\left(y_t - \sum_{k=0}^{m} f_k x_{t-k}\right)\left(-x_{t-j}\right)\right\} \\
&= 2E\left\{\sum_{k=0}^{m} f_k x_{t-k} x_{t-j} - y_t x_{t-j}\right\} \\
&= 2\left[\sum_{k=0}^{m} f_k E\left(x_{t-k} x_{t-j}\right) - E\left(y_t x_{t-j}\right)\right] \\
&= 2\left[\sum_{k=0}^{m} f_k \phi_{xx}(j-k) - \phi_{yx}(j)\right]
\end{aligned}
\tag{53}
$$

Where in the last equation we used the definition of auto-correlation and cross-correlation functions:

$$
\begin{aligned}
\phi_{xx}(k) &= E\left\{x_{t+k} x_t\right\} \\
\phi_{xy}(k) &= E\left\{x_{t+k} y_t\right\}
\end{aligned}
\tag{54}
$$

Hence, from the above we get the *normal equations*:

$$
\sum_{k=0}^{m} f_k \phi_{xx}(j-k) = \phi_{yx}(j) \qquad j = 0,1,\ldots,m \tag{55}
$$

Thus, to calculate the filter coefficients, we have to solve the set of normal equations in (55). The quantities we have to compute in order to be able to solve these equations, and which are readily available from the data, are the auto-correlation of the input and the cross-correlation between the desired output and the input.

Now suppose that the desired output is a unit spike

$$y_t = \delta(t) = \begin{cases} 1 & \text{for } t = 0 \\ 0 & \text{for } t > 0 \end{cases} \tag{56}$$

We then get

$$\begin{aligned} \phi_{yx}(j) &= E\{y_{t+j} x_j\} \\ &= \frac{1}{N+1} \sum_{t=0}^{N} y_{t+j} x_t \\ &= \begin{cases} x_0 & \text{for } j = 0 \\ 0 & \text{for } j > 0 \end{cases} \end{aligned} \tag{57}$$

And so the normal equations become

$$\sum_{k=0}^{m} f_k \phi_{xx}(j-k) = \delta(j) \qquad j = 0,1,\ldots,m \tag{58}$$

(we normalized by x_0 here, which affects only the amplitude of the filter).

Setting $c_{j-k} = \phi_{xx}(j-k)$ and writing (58) in vector form, we get

$$\mathbf{Af} = \boldsymbol{\delta} \tag{59}$$

where $\boldsymbol{\delta} = (1,0,\ldots,0)^T$ and $\mathbf{A}$ is given by

$$\mathbf{A} = \begin{pmatrix} c_0 & c_1 & c_2 & \cdots & c_m \\ c_1 & c_0 & c_1 & \cdots & c_{m-1} \\ c_2 & c_1 & c_0 & \cdots & c_{m-2} \\ & & & \vdots & \\ c_m & c_{m-1} & c_{m-2} & \cdots & c_0 \end{pmatrix} \tag{60}$$

A matrix of this special form, i.e. where each diagonal consists of the same elements, is called a Toeplitz matrix. Solving a system of equations based on such a matrix can be done using the Levinson recursion method in a much

more efficient manner than for an arbitrary matrix. This procedure is documented in most standard textbooks (e.g. Press *et al.*, 1988; Robinson and Treitel, 1980) and will not be repeated here. The code given below, however, does include a computer implementation of the procedure, written in MATLAB.

```
function f = normeq(m, r, g)
%  NORMEQ(M,R,G)
%  MATLAB function that solves the normal
%  equations to produce a filter of length M.
%  R and G are the auto-correlation and
%  cross-correlation vectors, respectively.

%  The procedure here follows the one outlined
%  in by Robinson and Treitel, 1980, with some
%  modifications to take advantage of MATLAB's
%  handling of vectors.

%  Make sure we have row vectors.

r = r(:)';
g = g(:)';

%  Initial conditions for the recursion.

ap(1) = 1;
u = r(1);
v = r(2);
f(1) = g(1)/r(1);
w = f(1)*r(2);

%  Use only the data that we need for the
%  computations.

r=r(1:m);
g=g(1:m);

%  Main recursive loop. It is recursive
%  mathematical-wise, not computer-wise.

for n = 1:m-1

  k = -v/u;
  a(1) = ap(1);
```

```
  for i = 2:n
    a(i) = ap(i)+k*ap(n+2-i);
  end

  a(n+1) = k*ap(1);
  u = u+k*v;
  q = (g(n+1)-w)/u;

  f(n+1) = 0;
  f = f+q*fliplr(a);

  if n < m-1

%  fliplr is a built-in function that flips
%  a matrix in the left/right direction.

    v = a*[fliplr(r(2:n+2))]';
    w = f*[fliplr(r(2:n+2))]';
    ap = a;

  end

end

f = f(:);

%  End
```

The following MATLAB code calculates the conventional Weiner deconvolution filter by calling the function given above.

```
function a = c_dcon(n, x)
%  C_DCON(N,X)
%  Calculates the coefficients of the
%  conventional deconvolution filter of
%  length n for a trace x.

%  Calculate the auto-correlation vector
%  for the trace. Corr is a built-in function.

for k = 1:n
  r(k,1) = corr(x,k-1);
end
```

```
%  Generate the right-hand-side (delta).

g = [1; zeros(n-1,1)];

%  Calculate the filter by solving the
%  normal equations. See above.

a = normeq(n,r,g);

%  End
```

The following MATLAB code calculates the generalized Weiner deconvolution filter as outlined earlier in the main body of the thesis.

```
function a = g_dcon(n, x, d)
%  G_DCON(N,X,D)
%  Calculates the coefficients of the
%  generalized deconvolution filter of
%  length n for a trace x where the
%  reflection are assumed to have a
%  correlation structure governed by a
%  fractionally integrated noise process
%  of order d.

%  Generate the right-hand-side (delta).

g = [1; zeros(n-1,1)];

%  Calculate the auto-correlation function
%  of the fractionally integrated noise
%  process. This function is given later.

r = accmfin(d,n-1);

%  Solve the normal equation to produce an
%  inverse filter for the reflection
%  coefficients.

f1 = normeq(n,r,g);

%  Apply the filter to the trace.

w = conv(f1,x);
```

```
%  Calculate the auto-correlation vector
%  for the output of the previous inverse
%  filter. Corr is a built-in function.

for i = 1:n
  r(i,1) = corr(w,i-1);
end

%  Calculate the generalized filter by solving
%  the normal equations. See above.

a = normeq(n,r,g);

%  End
```

The following function calculates recursively the auto-correlation function of a fractionally integrated noise process, taking advantage of the special form of the auto-correlation function.

```
function acc = accmfin(d,l)
%  accmfin(D,L)
%  Calculates the auto-correlation
%  function of a fractionally integrated
%  noise process of order d, up to lag l.

%  If nothing to do, return.

if l == 0
  acf = 1;
  return;
end

%  Initialize the recursion.

acc(1) = 1;

%  Main recursive loop. It is recursive
%  mathematical-wise, not computer-wise.

for k = 1:l
  acc(k+1) = acc(k)*(k+d-1)/(k-d);
end

acc=acc(:);
```

```
%  End
```